Parallel Peptide Actions Underlie Recruitment and Coordination of a Dual-Network Neuron

Savanna-Rae H Fahoum

Dawn M Blitz

Abbreviated Title: Parallel Peptide Actions for Dual-Network Activity

Department of Biology
Center for Neuroscience and Behavior
Miami University
Oxford OH 45056

[1]Corresponding Author:
Dawn M. Blitz
700 E High St
PSN 212
Oxford OH, 45056
blitzdm@miamoh.edu
513-529-6327

Number of pages: 80
Number of figures: 11 (+ 5 Extended data figures)
Number of tables: 2
Number of words
- Abstract: 243
- Significance Statement: 118
- Introduction: 647
- Discussion: 1495

Conflict of Interest: The authors declare no competing financial interests.

Acknowledgements: This work supported by the National Science Foundation IOS:1755283 (DMB).

Abstract

Oscillatory networks underlying rhythmic motor behaviors, and sensory and complex neural processing, are flexible, even in their neuronal composition. Neuromodulatory inputs elicit neuronal switching, whereby neurons switch participation between networks, or into multiple networks simultaneously. In most examples of neuronal switching, recruitment and coordination occur via the same mechanism, neuromodulation of internetwork synapses. However, separate mechanisms could enable additional flexibility. Here we explored whether modulation of synaptic properties occurs for a neuron recruited into dual-network activity via modulation of intrinsic properties. The isolated stomatogastric nervous system of the crab, *Cancer borealis,* contains two well-defined feeding-related networks (pyloric, food filtering, ~1 Hz; gastric mill, food chewing, ~0.1 Hz). The projection neuron MCN5 uses the neuropeptide Gly^1-SIFamide to recruit the typically pyloric-only LPG neuron into dual pyloric plus gastric mill-timed bursting via modulation of LPG intrinsic properties. However, modulation of LPG intrinsic properties is insufficient for coordinating LPG with the gastric mill network, because synapses between LPG and gastric mill neurons are not effective under baseline conditions. Here, we show that LPG and gastric mill neurons IC, LG, and DG entrain each other during Gly^1-SIFamide application, indicating bidirectional, functional connectivity. Further, in two-electrode voltage clamp recordings, Gly^1-SIFamide enhanced bidirectional graded inhibitory synaptic currents between LPG and LG, IC, and DG. Thus, a neuropeptide that recruits a switching neuron into dual-frequency oscillations also modulates synapses that enable network coordination. These parallel

modulatory actions provide the possibility of independent regulation of recruitment and coordination for neuronal switching.

Significance Statement

Neurons can exhibit activity that is simultaneously coordinated with separate networks. In previous examples where such a neuron was recruited into a second network, the recruitment occurred via modulation of internetwork synapses, which also coordinated activity of the switching neuron with the second network. In an alternative scenario where recruitment occurs via peptidergic modulation of intrinsic ionic currents instead of internetwork synapses, we find that peptidergic modulation of synapses between the recruited neuron and members of the second network also occurs for coordination of the switching neuron with the second network activity pattern. Thus, we determine that recruiting a neuron into a second network and coordinating its activity with the new network can occur via independent modulatory actions.

Introduction

Central pattern generators (CPGs) are flexible neuronal networks that produce different versions of rhythmic motor behaviors such as walking, breathing, and chewing (Bucher et al., 2015; Grillner & Kozlov, 2021; Leiras et al., 2022; Doi & Ramirez, 2008; Devineni & Scaplen, 2022). CPG flexibility includes neuronal switching, in which a neuron changes participation from its “home” network into another, or multiple networks simultaneously, via neuromodulation of synaptic and/or intrinsic properties (Hooper & Moulins, 1990; Weimann et al., 1991; Meyrand et al., 1994; Dickinson, 1995; Tryba et al., 2008; Drion et al., 2019; Fahoum and Blitz, 2021). Neuronal switching occurs in invertebrate and vertebrate CPG motor networks, other local oscillatory networks such as in the hippocampus, and is proposed to contribute to larger-scale changes in functional connectivity (Buzsáki and Draguhn, 2004; Bouret and Sara, 2005; Tryba et al., 2008; Kopell et al., 2014; Rangel et al., 2016; van den Brink, 2019; Fahoum and Blitz, 2021; Higley and Cardin, 2022). Neuromodulator inputs such as cholinergic basal forebrain and locus coeruleus neurons are implicated in regulating network dynamics on multiple temporal and spatial scales (Bouret and Sara, 2005; Kopell et al., 2014; van den Brink, 2019; Lohani et al., 2022). To fully understand how neuromodulatory inputs alter neuronal participation, it is necessary to identify the full complement of modulatory actions enabling a switching neuron to generate activity at the same frequency as a new network and with the correct timing relative to other neurons for meaningful network and behavioral output. However, determining the cellular-level mechanisms by which modulatory neurons alter intrinsic and synaptic properties to recruit and coordinate switching neurons can be difficult in large, diffuse networks.

Small invertebrate CPGs with identified modulatory inputs facilitate investigation of cellular mechanisms of neuronal switching. In several examples, modulation of internetwork synapses onto the switching neuron recruits a neuron to generate activity at the correct frequency and also enables the correct relative timing (Hooper and Moulins, 1990; Meyrand et al., 1994; Dickinson, et al., 1990). In such instances, the switching neuron is typically a passive member of its new network. More recent examples indicate that modulation of intrinsic properties can also regulate neuronal switching (Drion et al. 2019; Tryba et al., 2008; Fahoum and Blitz, 2021). We recently found that a neuron recruited to generate activity at a second network frequency via modulation of intrinsic properties can coordinate the relative timing of second network neurons, and this active role cannot be explained by modulation of intrinsic properties. Thus, we examined whether modulation of synaptic properties additionally impacts the same switching neuron in which intrinsic properties are modulated.

In the STNS of the crab, *Cancer borealis*, activation of the modulatory commissural neuron 5 (MCN5) causes the pyloric-only LPG neuron to switch into simultaneous dual pyloric- plus gastric mill-timed bursting (fast plus slow bursting, respectively) (Fahoum & Blitz, 2021). The LPG switch into slow bursting occurs due to modulation of LPG intrinsic properties via the MCN5 neuropeptide Gly^1-SIFamide (Fahoum & Blitz, 2021; Snyder & Blitz, 2022). As part of our investigation into how the MCN5-elicited rhythm is generated, we found that LPG gastric mill-timed (slow) bursting is regulated by gastric mill network neurons, and that LPG can contribute to coordination among gastric mill network neurons (Fahoum and Blitz, 2023), suggesting bidirectional communication between the LPG switching neuron and at least some of

the gastric mill network neurons. However, in baseline conditions LPG and LG, IC, and DG gastric mill neurons do not exhibit functional connections. Therefore, we hypothesized that in addition to modulating LPG intrinsic properties, the neuropeptide Gly^1-SIFamide also modulates synaptic transmission between LPG and LG, IC, and DG neurons. To test this, we assessed the ability of LPG, LG, IC, and DG to entrain the other neurons, and used two-electrode voltage clamp recordings to examine whether Gly^1-SIFamide modulated synapses between the switching neuron LPG and the gastric mill neurons IC, LG, and DG.

Materials and methods

Animals

Male *Cancer borealis* crabs were obtained from The Fresh Lobster company (Gloucester, MA) and maintained in tanks containing artificial seawater at 10-12 °C. For experiments, crabs were anesthetized on ice for 30-50 mins, then during gross dissection, the foregut was removed from the animal, bisected, and pinned flat in a Slygard-170-lined dish (Thermo Fisher Scientific). During fine dissection, the stomatogastric nervous system (STNS) was dissected from the foregut and pinned in a Sylgard 184-lined petri dish (Thermo Fisher Scientific) (Gutierrez and Grashow, 2009). During the dissection, the preparation was kept chilled in *C. borealis* physiological saline at 4 °C.

Solutions

C. borealis physiological saline was composed of the following (in mM): 440 NaCl, 26 $MgCl_2$,13 $CaCl_2$,11 KCl,10 Trizma base, 5 Maleic acid, pH 7.4-7.6. Squid internal electrode solution contained the following (in mM): 10 $MgCl_2$, 400 Potassium D-gluconic acid, 10 HEPES, 15 $NaSO_4$, 20 NaCl, pH 7.45 (Hooper et al., 2015). Gly^1-SIFamide (GYRKPPFNG-SIFamide, custom peptide synthesis: Genscript) (Huybrechts et al., 2003; Yasuda et al., 2004; Dickinson et al., 2008; Blitz et al., 2019; Fahoum and Blitz, 2021) was dissolved in optima water (Thermo Fisher Scientific) at 10^{-2} M and stored at -20 °C. Tetrodotoxin (TTX) powder was dissolved in optima water at a final concentration of 10^{-4} M and stored at -20 °C. Stock solution of picrotoxin (PTX) was made by directly adding PTX powder (Sigma Aldrich) to 95% ethanol at 10^{-2} M and storing at -20 °C. For experiments, each substance was thawed and diluted in physiological saline at a final concentration of: Gly^1-SIFamide, 5 µM; TTX, 1 µM and 0.1 µM; PTX, 10 µM.

Electrophysiology

All preparations were continuously superfused with chilled *C. borealis* saline (8-10 °C), or chilled saline containing Gly^1-SIFamide, PTX, and/or TTX, as indicated. For uninterrupted superfusion of the preparation, all solution changes were performed using a switching manifold. Extracellular nerve activity was recorded using a model 1700 A-M Systems Amplifier and custom-made stainless-steel pin electrodes. Vaseline wells were built around nerves to isolate neuron signals, with one stainless-steel electrode wire placed inside the well, and the other outside the well as reference. Stomatogastric

ganglion (STG) somata were exposed by removing the thin layer of tissue across the ganglion and observed with light transmitted through a dark-field condenser (MBL-12010 Nikon Instruments). Intracellular recordings were collected using sharp-tip glass microelectrodes (18-40 MΩ) filled with squid internal electrode solution for entrainment experiments or filled with 0.6 M K_2SO_4 plus 20 mM KCl electrode solution for voltage clamp experiments. STG neurons and their locations were identified based on their intracellular activity, nerve projection patterns, and their interactions with other STG neurons. All intracellular recordings were collected using AxoClamp 900A amplifiers in current-clamp mode for entrainment experiments or two-electrode voltage clamp (TEVC)-mode for synapse experiments (Molecular Devices). All experiments were conducted in the isolated STNS following transection of the inferior and superior oesophageal nerves (*ion* and *son*, respectively). Electrophysiology recordings were collected using data acquisition hardware (Entrainment experiments: Micro1401, Cambridge Electronic Design; Synapse experiments: DigiData 1440A, Molecular Devices), software (Entrainment experiments: Spike2, ~5 kHz sampling rate, Cambridge Electronic Design; Synapse experiments: Clampex 10.7, Molecular Devices, 5 kHz sampling rate) and laboratory computer (Dell).

Prior to all conducted experiments, unless otherwise indicated, the LP neuron was photoinactivated as described in Fahoum and Blitz (2021). Briefly, the LP neuron was impaled with a sharp microelectrode (30-40 MΩ) that was tip-filled with AlexaFluor-568 hydrazide (10 mM in 200 mM KCl, Thermo Fisher Scientific) and back-filled with squid internal solution (*see Solutions*). The LP soma was filled using constant hyperpolarizing current injection (-5 nA) for 5-10 mins, and the current injection removed

to allow the dye to diffuse to the neurites and axon in the *dvn* for 20-40 mins. The STG was then illuminated for 5-7 mins using a Texas red filter set (560 ± 40 nm wavelength; Leica Microsystems). Complete photoinactivation was confirmed when the LP membrane potential reached 0 mV.

Gastric mill network entrainment

To examine whether each gastric mill-timed network neuron (LPG [two copies], LG, IC, and DG [one copy each]) entrained each other, entrainment neurons (LPG, LG, IC, or DG) were stimulated with rhythmic depolarizing current injections (5 s pulse duration, +0.5 to 6 nA) at different entrainment frequencies (in Hz: 0.03, 0.06, 0.075, 0.09, 0.12; i.e., 5 s pulse, 6 to 28 sec inter-pulse interval). In some cases, the baseline burst frequency of the entrainment neuron was faster than the slowest (0.03 Hz) entrainment frequency, such that extra bursts occurred between stimulations. Thus, we increased the entrainment frequency by 0.01 Hz until bursting activity of the entrainment neuron only occurred during each depolarizing stimulation. Stimulation frequencies in which there were spontaneous entrainment neuron bursts between depolarizing stimulations were not included in the analysis. The amount of current injected into the entrainment neuron was chosen to match the baseline firing frequency (± 5 Hz) of that neuron at steady state Gly^1-SIFamide application prior to initiating entrainment depolarizations. In some preparations, the entrainment neuron was not active at baseline conditions, thus, we used the mean firing frequency of the entrainment neuron from other preparations to select the appropriate amount of current to inject. All entrainment manipulations were conducted during the last 20 mins of a 30-min Gly^1-

SIFamide (5 µM) application. To examine LPG entrainment of gastric mill neurons LG, IC, and DG more directly, we performed an additional set of experiments where we combined picrotoxin (PTX, 10 µM), which blocks LG, IC, and DG glutamatergic inhibitory synapses, but not cholinergic LPG synapses (Marder, 1974, 1976; Hooper et al., 1986), with Gly^1-SIFamide (SIF:PTX). This condition isolates LPG from gastric mill input and leaves LPG as the only functional chemical synapse among the LG, IC, DG, and LPG group.

For each entrainment frequency, the entrainment neuron (LG, IC, DG, or 2 LPGs) was rhythmically depolarized for ten cycles (11 bursts), and the instantaneous slow burst frequency (1/cycle period [time between the first action potentials of two consecutive bursts]) for each test neuron (LG, IC, DG, and LPG) was measured. Depending on whether the test neuron was entrained or not, and whether it was entrained one-to-one (1:1) or with other relationships such as one-to-two (1:2, one test neuron burst per two entrainment bursts), there were variable numbers of slow bursts for test neurons across frequencies and preparations as indicated in the Results section. Only gastric mill-timed bursts (defined below in Gastric mill burst identification) were measured for LPG and IC neurons which can participate in both the pyloric and gastric mill rhythms. We report individual instantaneous slow burst frequencies of each set of test neuron bursts (variable number) in response to 10 entrainment cycles (11 bursts).

Integer coupling analysis

To quantify the extent of entrainment between LG and IC, DG, and LPG, we used integer coupling as a measure of whether there was a fixed relationship between the burst frequencies of each pair of neurons (Nadim et al., 1998; Bucher et al., 2006; Powell et al., 2021). Integer coupling was measured by dividing the entrainment neuron stimulation frequency by the instantaneous test neuron burst frequency and extracting the significand (the value to the right of the decimal point) from each ratio at each entrainment frequency, across preparations. The significand indicates a measure of how close a ratio is to an integer. For instance, if the ratio between the entrainment and instantaneous burst frequencies is 1.01, then significand is 0.01 and close to zero. If the ratio is 1.99, then the significand is 0.99 and close to 1. The cumulative probability distribution frequency (c.d.f.) of all significands for each entrainment frequency was calculated to determine how close each set of ratios was to an integer and plotted on a histogram. The shaded regions in Figures 2-6D indicate the c.d.f. curves between entrainment and test neurons at 0.06 Hz entrainment frequency. The blue dotted line in Figures 2-6D indicates one extreme of perfect integer coupling, where all significands from all ratios are near 0 or 1, and the c.d.f. accumulates primarily at 0 or 1 (Powell et al., 2021). On the other hand, if all significands across a group of data points are randomly and uniformly distributed between 0 and 1, then the c.d.f. of these values would be close to a diagonal line, and thus indicate zero integer coupling between neurons (solid red y = x line, Figs. 2-6D) (Nadim et al., 1998; Powell et al., 2021).

To quantify the extent of integer coupling at each entrainment frequency, that is, the distance between the cumulative distribution and a random distribution (i.e., a

diagonal line), we calculated the area between each c.d.f. curve and the diagonal line using a custom-written MATLAB script (MathWorks). For instance, if there was perfect integer coupling at a particular entrainment frequency, then the area between a c.d.f. falling along the dotted line and the diagonal would be 0.25, while an area closer to zero would suggest there is no integer coupling between the entrainment and test neurons. To determine whether significands from a group of entrainment frequencies were significantly different from the diagonal line, we formulated a uniform distribution that would equal the y = x diagonal line, and thus have an area equal to zero to indicate no integer coupling. Then, for each entrainment frequency, we compared the experimental data to the uniform distribution using a two-sample Kolmogorov-Smirnov test (Powell et al., 2021). We used a two-sample test instead of a one-sample test because the calculated significands for the experimental data cannot be expected to be normally distributed (Powell et al., 2021). We divided the significance level by the number of entrainment frequencies (7) to correct for multiple comparisons. Thus, our significance threshold was 0.05/7 = 0.007. Entrainment frequencies with only one preparation tested were excluded from the integer coupling analysis.

<u>Gastric mill neuron burst identification</u>

Only neurons that were bursting in gastric mill time during entrainment stimulations were included in the entrainment plots and integer coupling analysis. Criteria to determine gastric mill-timed bursting included: IC bursts had a duration of at least 0.45 s (Blitz et al., 2019; Fahoum and Blitz, 2023); LG and DG bursts had at least 3 spikes per burst and a maximum 2 s interburst interval; and LPG gastric mill-timed

bursts were identified as described in Fahoum and Blitz, 2021. Briefly, a histogram containing LPG interspike intervals (ISIs) across an entire Gly^1-SIFamide application was generated using a custom-written MATLAB script and the two largest peaks identified. The mean ISI between the first peak (~0-0.5 s, intraburst intervals [interval between spikes during a burst]) and second peak (~0.5-2 s, interburst intervals [interval between spikes between bursts]) was calculated and used as a cutoff value to identify LPG bursts, such that an ISI above the cutoff indicated the end of one burst and the beginning of another. A custom written Spike2 script that identifies LPG bursts with a duration greater than one pyloric cycle period (from PD burst onset to the next PD burst onset, ~1 s) was then used to select only LPG slow bursts from all LPG bursts identified with the ISI cutoff (Fahoum & Blitz, 2021).

Graded synapses via two-electrode voltage clamp

To determine whether graded synapses between LPG and gastric mill neurons were modulated by Gly^1-SIFamide, we used two-electrode voltage clamp (TEVC) recordings. Based on previous studies, we only proceeded with experiments and analyzed data when pre- and post-synaptic cells had an input resistance of at least 10 MΩ (Hooper et al., 2015; Schneider et al., 2021). Action potentials were blocked with TTX (initial concentration: 1 µM, ~5-10 mins; final maintained concentration: 0.1 µM). When IC, LG, or DG was the presynaptic neuron, they were voltage clamped at -60 mV. The presynaptic neuron was stepped from its holding potential to -55 to -20 mV in 5 mV increments (5 s duration, 11 s inter-step interval). The postsynaptic cell was voltage clamped at -40 mV. For IC, LG, and DG to LPG synapses, the voltage step protocol

was repeated in Gly^1-SIFamide (SIF, 5 µM) plus TTX (0.1 µM) (TTX:SIF), following ~10 mins wash-in of TTX:SIF. To measure potential LPG to IC, LG, or DG synapses, the same voltage step protocol was used, however, PTX (10 µM) was used to block glutamatergic inhibitory synapses. LPG uses acetylcholine as its transmitter, and thus its actions are not blocked by PTX (Marder, 1974, 1976; King, 1976; Hooper et al., 1986), enabling us to examine synapses from LPG onto LG, IC, and DG more directly in TTX:Saline versus TTX:SIF. When LPG was the presynaptic neuron, it was held at -80 mV to turn off spontaneous activity of the other non-clamped LPG neuron. LPG was stepped from its holding potential to -55 mV to -20 mV in 5 mV increments, and the postsynaptic neuron current recorded with cells at a holding potential of -40 mV. This protocol was repeated in Gly^1-SIFamide (5 µM) plus TTX (10^{-7} M) plus PTX (10^{-5} M) (TTX:PTX:SIF), following ~10 mins wash-in of TTX:PTX:SIF. In a small subset of experiments as indicated, each presynaptic neuron (LG, IC, DG, or LPG), was clamped at a holding potential of -80 mV and stepped from -70 mV to -20 mV in 5 mV increments. Between each experimental condition, all neurons were held at -60 mV, near resting potential for STG neurons (Martinez et al., 2019). Due to a factor of 10 error in a gain setting in TEVC in one amplifier, current amplitudes were multiplied post-hoc by a factor of 10. Before any adjustments were made, input resistance measurements in current clamp mode, unaffected by the gain error, from pre- and post-TEVC mode were compared to input resistance measurements in TEVC mode to verify the gain factor error. Additionally, the same neuron (e.g., LG) was not always recorded using the channel with the gain error from preparation to preparation. Adjusted data matched the data recorded with the correct conversion factor.

Voltage step protocols were repeated 5 times in each direction during each pair of synapses tested. Recordings were averaged and filtered using Clampfit 10.7 (pClamp, Molecular Devices, San Jose, CA) prior to analysis. Synaptic currents were measured by subtracting the mean holding current during the 2 s preceding each voltage step from the peak current at each of three timepoints: (1) the first 2 s of the voltage step (First); (2) the last 2 s of the voltage step (Last); (3) the first 2 s after the voltage step (Post). For LPG to IC and to LG, we observed an inward current within the first 2 s of each voltage step. Thus, we also measured the peak amplitude of this inward current and subtracted it from the mean holding current.

Software and Statistics

Raw electrophysiology data were analyzed using Clampfit 10.7, as well as functions and scripts that were written in Spike2 and MATLAB. Graphs were plotted in SigmaPlot or MATLAB and imported into CorelDraw. All final figures were created using CorelDraw (Corel). Statistical analyses were performed using SigmaPlot (Systat) or MATLAB. Data were analyzed for normality using Shapiro-Wilk test before determining whether to use a parametric or nonparametric test on each dataset. A two-sample Kolmogorov-Smirnov test was used for integer coupling analysis. Two-way repeated measures (RM) analysis of variance (ANOVA) and Holm-Sidak post hoc tests for multiple comparisons were used for synaptic current analyses. Threshold for significance was $p < 0.05$, except for integer coupling analysis which had a threshold of $p < 0.007$. All data are presented as mean ± SEM.

Code Accessibility

Scripts and functions used for analysis were written in Spike2 and/or MATLAB and are available at https://github.com/blitzdm/Fahoum_Blitz_2023_Synapses or upon request from D.M.B.

Results

The isolated stomatogastric nervous system (STNS) is a region of the crab, *Cancer borealis*, nervous system that controls pyloric (food filtering, ~1 Hz) and gastric mill (food chewing, ~0.1 Hz) feeding behaviors (Nusbaum & Beenhakker, 2002; Daur et al., 2016) (Fig. 1A). The STNS is comprised of the paired commissural ganglia (CoG), single oesophageal ganglion (OG), and the single stomatogastric ganglion (STG), and their connecting and peripheral nerves (Fig. 1A). The STG contains ~30 neurons that are interconnected to form well-characterized CPG networks which drive the pyloric and gastric mill rhythms. The CoGs and OG contain modulatory projection neurons that project to the STG and activate and modulate the pyloric and gastric mill CPGs (Blitz, 2023). The pyloric pacemaker interneuron, anterior burster (AB), is electrically coupled to the pyloric dilator (PD, 2 copies) and lateral posterior gastric (LPG, 2 copies) motor neurons, and together they form the pacemaker group for the pyloric rhythm (Marder & Eisen, 1984; Shruti et al., 2014) (Fig. 1B). The interneuron 1 (Int1) and lateral gastric (LG) neurons are connected via reciprocal glutamatergic chemical inhibition and, together, form the rhythm generator for the gastric mill rhythm (Coleman et al., 1995; White and Nusbaum, 2011) (Fig. 1B). Multiple versions of the pyloric and gastric mill rhythms are generated via neuromodulation of intrinsic properties of individual neurons

and/or the synapses between them (Blitz 2023; Nadim and Bucher, 2014; Stein, 2009). The projection neuron modulatory commissural neuron 5 (MCN5) is located in the CoG and projects its axons to the STG via the inferior oesophageal and stomatogastric nerves (*ion* and *stn*, respectively; Fig. 1A). Bath application or neuronal release of the MCN5 neuropeptide Gly^1-SIFamide increases pyloric frequency (Norris et al., 1996) and activates the gastric mill rhythm (Fahoum and Blitz, 2021; Blitz et al., 2019). Furthermore, MCN5 activation or bath application of its neuropeptide Gly^1-SIFamide (5 µM) switches the pyloric-only LPG neuron into dual pyloric/gastric mill-timed bursting (fast/slow, respectively) (Blitz et al., 2019; Fahoum & Blitz, 2021). LPG generates slower bursts in the gastric mill frequency range due to modulation of LPG intrinsic properties (Fahoum & Blitz, 2021; Snyder & Blitz, 2022). Although the LPG gastric mill-timed (slow) bursting does not require synaptic input from the gastric mill network, these oscillations are regulated by gastric mill network neurons including being coordinated with the rest of the gastric mill network. Further, LPG slow bursting regulates LG and dorsal gastric (DG) neuron activity, and LPG can coordinate gastric mill network neurons (Fahoum and Blitz, 2023). The baseline connectome does not include functional synapses to explain interactions between LPG and gastric mill network neurons (Fig. 1B) (Marder and Bucher, 2007). Thus, we hypothesize that Gly^1-SIFamide modulates synapses between LPG and LG, IC, and DG to enable interactions between the switching neuron LPG and other gastric mill neurons, LG, IC, and DG.

Entrainment

We first investigated whether functional connections were present between LPG, LG, IC, and DG neurons during Gly^1-SIFamide application by testing whether imposing a range of burst frequencies onto each neuron entrained the burst frequency of the other neurons (Figs. 2 – 6). For this approach, we injected rhythmic depolarizing current into each entrainment neuron (LG, IC, DG, or LPG) across a range of frequencies (0.03 – 0.12 Hz; see Methods) and evaluated the slow network bursting of the other gastric mill neurons.

LG entrainment of IC, DG, and LPG

We first examined whether LG could entrain IC, DG, and LPG neurons in Gly^1-SIFamide (5 µM, Fig. 2). In an example experiment, prior to any manipulations, LG was bursting at approximately 0.03 Hz and IC, DG, and LPG were bursting in a relatively coordinated manner (Fig. 2Ai-Ci, Baseline). For clarity, for all entrainment frequencies presented, we use upward arrowheads to indicate the onset of each entrained neuron burst and only show recordings of the test neurons. When LG was stimulated with an entrainment frequency of 0.06 Hz (upward arrowheads), IC generated a slow burst with each LG stimulation (Fig. 2Aii). As LG entrainment frequency was increased, IC continued to generate 1-2 slow bursts within each LG stimulation cycle, with two slow IC bursts triggered by an LG stimulation more frequently at higher entrainment frequencies (Fig. 2Aii). DG bursts overlapped with LG bursts at baseline, except for one LG cycle, where DG burst twice within the cycle (Fig. 2Bi, Baseline, dotted line). However, when the LG entrainment frequency was increased from 0.06 Hz to 0.09 Hz, DG generated

one burst for every two LG cycles (Fig. 2Bii). At 0.12 Hz entrainment frequency, DG burst frequency slowed further, such that DG generated one burst for every four LG cycles (Fig. 2Bii). Thus, although DG bursts occurred at a lower frequency than the entrainment frequency (0.06 – 0.12 Hz), DG was coordinated with LG at higher entrainment frequencies but not in a 1:1 relationship. Finally, for LG and LPG slow bursting, at baseline, LPG typically generated one burst per LG cycle, except for one cycle where LPG generated two slow bursts (Fig. 2Ci, Baseline). As the LG entrainment frequency was increased from 0.06 Hz to 0.12 Hz, LPG appeared to maintain 1:1 coordinated slow bursting (Fig. 2Cii). At 0.12 Hz LG entrainment frequency, a 1:1 relationship between LPG and LG persisted, although the relative timing between each LPG burst and the onset of the LG bursts was less consistent than at lower entrainment frequencies (Fig. 2Cii, 0.12Hz). LG does regulate LPG slow burst cycle period (Fahoum and Blitz 2023). The example experiment shown indicates that LG was able to entrain LPG within a range of frequencies (0.06 – 0.09 Hz), whereas above that, LG regulated the LPG cycle period but was not able to entrain LPG bursting.

Across preparations, to determine whether IC, DG, and LPG neurons were entrained to the imposed LG entrainment frequencies, we measured instantaneous burst frequency of all test neuron bursts, in all preparations and plotted those values against LG entrainment frequency (Fig. 2Aiii-Ciii). Each color represents one preparation. For LG and IC, the data points from each preparation clustered mostly on the solid diagonal line (Fig. 2Aiii). For instance, at 0.06 Hz, 0.075 Hz, and 0.09 Hz there are a total of 71, 48, and 71 cycles plotted, respectively. However, these data points are largely overlapping due to their entrainment by LG at these frequencies. The solid

diagonal line represents a 1:1 mode of entrainment, such that IC burst frequency was almost equal to LG entrainment frequency, indicating that LG entrained IC (Fig. 2Aiii; n = 3-7, Table 1). However, in some instances, IC did not burst in a 1:1 manner across entrainment frequencies, as evidenced by the vertical spread of data points, e.g., at 0.06 Hz and 0.12 Hz (Fig. 2Aiii). As described above, it was possible for a neuron to be coordinated with the entrainment neuron, but at a relationship different from 1:1. Thus, we plotted additional diagonal lines for other modes of entrainment, which indicate that the test neuron burst frequency was some multiple (or fraction) of the entrainment frequency (Fig. 2Aiii, dashed diagonal lines, see Methods). The addition of these lines enabled us to determine whether the data points not clustered on the 1:1 diagonal line were still entrained to the LG frequency by clustering at another entrainment mode, or perhaps not entrained if spread between entrainment modes. For instance, at 0.06 Hz, data points for instantaneous IC burst frequencies clustered primarily near the 1:1 line (64/70 data points). However, the additional points fell near the 1:2 (2/70), 4:1 (1/70), or 5:1 (3/70) lines, indicating that even if it was not a 1:1 relationship for every IC burst, IC activity was linked to that of LG and therefore was entrained by LG at 0.06 Hz. Conversely, at 0.12 Hz, while some data points fall on integer lines, many fall between them, indicating that IC was not readily entrained by LG at this frequency (Fig. 2Aiii).

For LG and DG, there was a range of instantaneous DG burst frequencies at each LG entrainment frequency (Fig. 2Biii; n = 2-7, Table 1). Unlike IC, DG coordination with LG entrainment frequency was not locked to primarily one mode of entrainment. For example, in one preparation (light blue data points), DG was entrained 1:1 at 0.05 Hz, but as LG entrainment frequency increased, DG burst frequency decreased such

that it maintained some coordination with LG in a 1:2 (0.06 – 0.09 Hz) and 1:3 (0.09 – 0.12 Hz) manner (Fig. 2Biii, light blue dots). This shift in entrainment mode occurred for some preparations (n = 5/7), although the direction of the shift was not consistent across individuals. DG did not appear to be entrained by LG at 0.06 Hz, due to the spread of data points between entrainment modes. However, it was a relatively small number of points (7/35 data points) that were spread between entrainment mode lines, the remainder of the data points clustered near 1:1 (12/35 data points), 1:2 (10/35), and 1:3 (6/35) lines. At the other entrainment frequencies, the instantaneous DG burst frequencies clustered mostly around entrainment modes, even at 0.12 Hz in 2/7 experiments (9/13 data points) (Fig. 2Biii). Thus, LG appeared to entrain DG, although not always in a 1:1 relationship (Fig. 2Bii).

For LG and LPG slow bursting, we observed a range of instantaneous LPG slow burst frequencies at most entrainment frequencies, except at 0.075 and 0.09 Hz (Fig. 2Ciii, n = 2-8, Table 1). Although some data points fell on entrainment mode lines, many points, across multiple experiments, were spread between entrainment modes between 0.03 and 0.06 Hz, and for 0.12 Hz (Fig. 2Ciii). However, at 0.075 and 0.09 Hz, LPG data points clustered on the 1:1 entrainment mode, with little variability, suggesting that LG can entrain LPG within a limited frequency range (Fig. 2Ciii). While these plots enabled a qualitative assessment of entrainment, we pursued a quantitative analysis as well.

<u>Integer coupling between LG and IC, DG, and LPG</u>

To quantify entrainment between LG and IC, DG, and LPG, we collapsed the data points at each entrainment frequency into a single value using an analysis of

integer coupling (Nadim et al., 1998; Bucher et al., 2006; Powell et al., 2021). Integer coupling was measured by first calculating the ratio between each instantaneous neuron burst frequency and the LG entrainment frequency across preparations for each entrainment frequency and then using the significands (value to the right of the decimal) from each set of ratios (i.e., IC/LG, DG/LG, LPG/LG) at each entrainment frequency to generate a cumulative probability distribution (c.d.f.) of significands (Fig. 2D; Extended Data Fig. 2-1). For a group of ratios, perfect integer coupling would result in all significands being 0 or 1. However, if there was no relationship between entrainment frequency and test neuron burst frequency, then the significands would be distributed relatively evenly between 0 and 1, resulting in a c.d.f. close to a diagonal line (y = x) (Fig. 2D, red diagonal line) (Nadim et al., 1998; Bucher et al., 2006; Powell et al., 2021). For the example entrainment frequency of 0.06 Hz, c.d.f.s of significands (bin size 0.01) for each of the test neurons are overlaid (Fig. 2D; IC, black; DG, dark grey; LPG, light grey; remaining entrainment frequency c.d.f.s in Extended Data Fig. 2-1). The blue dotted line indicates an extreme in which 50% of a theoretical significand distribution is 0 and 50% is 1, indicating perfect integer coupling (Fig. 2D, blue dotted line). In the c.d.f. for IC significands (black) ~70 % of significands were less than ~0.1 (Fig. 2D, black shape). This shape reflects the clustering of IC instantaneous burst frequency around the different entrainment modes at 0.06 Hz entrainment in the scatter plot (Fig. 2Aiii). The c.d.f. of DG significands indicates that fewer were close to 0 or 1 (Fig. 2D, dark grey). This reflects the spread of some DG data points between entrainment modes at 0.06 Hz in the scatter plot (Fig. 2Biii). The c.d.f. of LPG significands indicated even weaker integer coupling at 0.06 Hz entrainment frequency, with the distribution

being more similar to the diagonal line, demonstrating a relatively uniform distribution between 0 and 1 (Fig. 2D, light grey). This reflects the large spread of LPG data points across and between entrainment modes at 0.06 Hz (Fig. 2Ciii). Qualitatively, the c.d.f. histograms suggest that LG entrains IC more strongly than DG but does not entrain LPG at 0.06 Hz (Fig. 2D). Consistent with the scatter plots (Fig. 2Ciii), the c.d.f.s for LG to LPG entrainment at 0.075 and 0.09 indicate stronger integer coupling (Extended Data Fig. 2-1).

Once the c.d.f. for each test neuron, at each entrainment frequency (Fig. 2D; Extended Data Fig. 2-1), was determined, we calculated an overall measure of the extent of integer coupling at each entrainment frequency by calculating the area between each c.d.f. histogram and the diagonal line (no integer coupling) (Fig. 2D, shaded regions). These area measurements for each neuron were plotted against entrainment frequency, including from the example c.d.f.s for 0.06 Hz in figure 2D (Fig. 2E, downward arrow/dotted line). The dashed line at y = 0.25 indicates an example of perfect integer coupling, where test neuron burst frequency is equal to the entrainment neuron frequency, i.e., the area between the blue dotted line and the red diagonal line in figure 2D (Powell et al., 2021). Area values further from zero indicate integer coupling at that entrainment frequency. To determine whether the c.d.f. for each neuron at each entrainment frequency was significantly different from a uniform distribution (i.e., the diagonal line), we used a two-sample Kolmogorov-Smirnov test to compare each c.d.f. to a uniform distribution. A corrected significance level of 0.007 (see Methods) for the comparison between test neuron c.d.f. and a uniform distribution was used as the criterion for entrainment at a particular frequency. Results of this statistical analysis is

indicated above each entrainment frequency for each neuron (Fig. 2E). For instance, the area between the IC c.d.f. and the diagonal line at 0.03 Hz entrainment frequency was approximately 0.45 but the IC c.d.f. area decreased at higher entrainment frequencies (Fig. 2E, black line/symbols). Specifically, LG-to-IC integer coupling, and thus entrainment, occurred between 0.03 – 0.09 Hz ($p < 0.001$, $D > 0.43$), but not at 0.12 Hz ($p = 0.074$, $D = 0.18$). Although the area between c.d.f. and the diagonal line for DG was greater at an entrainment frequency of 0.05 and 0.075 Hz, than at other frequencies (Fig. 2E, dark grey line/circles), DG was entrained by LG at all entrainment frequencies (0.05 – 0.12 Hz, $p < 0.001$, $D > 0.32$). Finally, the area for LPG was below 0.25 across frequencies but was non-zero (Fig. 2E, light grey line/circles) and this area measurement was different from the uniform distribution at all entrainment frequencies ($p < 0.0012$, $D > 0.28$) except 0.06 Hz ($p = 0.03$, $D = 0.196$). Overall, these results indicate that IC, DG, and LPG were integer coupled to and entrained by LG to some extent, suggesting the presence of a functional synapse between these neurons in Gly^1-SIFamide.

This integer coupling analysis assumes test neuron integer-multiple relationships to the entrainment neuron (e.g., 1:1, 2:1, 3:1) using test neuron/entrainment neuron ratios. However, we did observe some fractional relationships in which there are fewer test neuron cycles relative to entrainment neuron (e.g., 1:2, 1:3; Fig. 2Biii). These entrainment relationships would result in significands between 0 and 1, for example a 1:2 entrainment would result in a significand of 0.5. The example “perfect” entrainment area of 0.25 (area between blue and red lines in figure 2D), represents equal proportions of significands occurring close to 0 or 1. Although the area calculation for

“perfect” entrainment at intermediate significand values would differ from 0.25, it should still be greater than 0 and thus we feel our area measurement enables us to quantify whether entrainment occurred, regardless of the type of entrainments.

Entrainment and integer coupling among the other gastric mill neurons

We found variability in the ability of IC, DG, and LPG to entrain the other neurons (Figs. 3 – 5). For instance, although LG entrained IC, IC did not appear to entrain LG. In the example shown, IC and LG gastric mill-timed bursting was coincident at baseline (Fig. 3Ai), but not when IC bursting was controlled with rhythmic current injections (Fig. 3Aii). Across experiments, data points were spread across a range of burst frequencies, with few points occurring along entrainment mode lines (Fig. 3Aiii; n = 2-6, Table 1). An example experiment suggested that IC might entrain DG at some frequencies, e.g., 1:2 at 0.075 Hz (Fig. 3Bii). However, in the full data set, data points for some experiments clustered along entrainment mode lines (e.g., red dots along 1:1 line) whereas data points for other experiments were spread across a range of frequencies (e.g., orange dots) (Fig. 3Biii; n = 3-8, Table 1). IC appeared to entrain LPG better at mid-level entrainment frequencies than at low or high frequencies at low or high entrainment frequencies (Fig. 3Cii-Ciii, n = 3-9, Table 1). Although there was some spread of the data points between entrainment modes, there was also clustering of LPG burst frequencies along some of the entrainment lines including 1:1. However, it is not clear in this plot how strong the entrainment was. For example, there are 80 and 65 data points at 0.06 and 0.075 Hz respectively, but it is difficult to assess how many are clustered at

the 1:1 entrainment line versus clumped together between entrainment mode lines. Thus, we again turned to integer coupling analysis (Fig. 3D-E).

IC appeared to most strongly entrain LPG, with weaker entrainment of DG and LG. At 0.06 Hz entrainment ~60% of LPG/IC significands were less than 0.1 (Fig. 3D, black shaded region; Extended Data Fig. 3-1). The c.d.f.s for DG (dark grey) and LG (light grey) were closer to the diagonal line, with ~25% and ~20% of significands less than 0.1, respectively (Fig. 3D). Across entrainment frequencies, LG was entrained by IC at 0.04, 0.06, and 0.12 Hz entrainment frequencies ($p < 0.007$, $D > 0.2$), but not at 0.05, 0.075, or 0.09 Hz (0.05 Hz, $p = 0.051$, $D = 0.186$; 0.075 Hz, $p = 0.051$, $D = 0.186$; 0.09 Hz, $p = 0.034$, $D = 0.196$). DG was entrained between 0.04 – 0.12 Hz ($p < 0.001$, $D > 0.27$), but not at 0.03 Hz entrainment frequency ($p = 0.271$, $D = 0.137$). Finally, LPG was entrained by IC at all entrainment frequencies ($p < 0.004$, $D > 0.24$). Thus, these results indicate that LG, DG, and LPG were all integer coupled to and entrained by IC at some entrainment frequencies, suggesting the presence of functional synapses from IC onto LG, DG, and LPG in the presence of Gly^1-SIFamide.

The DG neuron is the most likely to be uncoordinated with the other gastric mill neurons, or to be coordinated in modes other than 1:1 during the Gly^1-SIFamide gastric mill rhythm (Fahoum and Blitz, 2023). Despite this, stimulating DG across a range of entrainment frequencies revealed some degree of control over the burst frequency of the other neurons. For example, DG entrainment of LG was most apparent between 0.06-0.12 Hz (Fig. 4Aiii; n = 3-8, Table 1). IC instantaneous burst frequency appears quite variable, with a large spread of data points between entrainment modes (Fig. 4Biii; n = 2-8, Table 1). Nevertheless, DG appeared to entrain IC at 0.06-0.09 Hz frequencies,

with most data points clustered at entrainment modes (Fig. 4Biii). For LPG there was some clustering of burst frequencies, although across experiments the data points tended to spread beyond entrainment mode lines (Fig. 4Ciii; n = 3-11, Table 1). At a DG entrainment frequency of 0.06 Hz, ~75-80% of significands were less than 0.1 for LG and IC, while there were ~35% of significands less than 0.1 for LPG (Fig. 4D, shaded regions, LG (black); IC (dark grey); LPG (light grey) (additional c.d.f.s in Extended Data Fig. 4-1). The area between each c.d.f. and the diagonal line indicated that integer coupling was variable for DG to LG (black), IC (dark grey), and LPG (light grey) (Fig. 4E). LG and IC were entrained to DG at 0.03 and 0.05 – 0.12 Hz ($p < 0.001$, $D > 0.353$), but not entrained at 0.04 Hz (LG, $p = 0.356$, $D = 0.127$; IC, $p = 0.074$, $D = 0.177$). LPG was entrained by DG at 0.04 – 0.06 and 0.09 Hz ($p < 0.0012$, $D > 0.26$), but not entrained at 0.03, 0.075, or 0.12 Hz entrainment frequencies (0.03 Hz, $p = 0.022$, $D = 0.206$; 0.075 Hz, $p = 0.015$, $D = 0.216$; 0.12 Hz, $p = 0.051$, $D = 0.186$). These results indicate that LG, IC, and LPG were integer coupled to and entrained by DG to some extent, suggesting the presence of a functional synapse between these neurons during Gly^1-SIFamide application.

In the Gly^1-SIFamide modulatory state, LPG more strongly entrained the DG neuron compared to IC and LG. In example traces, it appears that LPG regulated the strength of the LG bursts, consistent with previous findings (Fahoum and Blitz, 2023). However, LPG did not appear to be very effective at entraining LG, or IC bursting (Fig. 5Aii-Aiii, 5Bii-Biii; Table 1). For LG and IC, many of the instantaneous burst frequencies were distributed between entrainment modes (Fig. 5Aiii, 5Biii). In example traces, DG burst frequency changed across entrainment frequencies but was only coordinated in a

1:1 manner at 0.06 Hz (Fig. 5Cii). Across experiments, there was clustering of DG burst frequencies along the 1:1 entrainment mode from 0.04 to 0.12 Hz with some spread of data points particularly from 0.075 to 0.12 Hz (Fig. 5Ciii; Table 1). This partial entrainment across experiments is further indicated by the c.d.f. histogram for DG at 0.06 Hz entrainment frequency, in which ~45% of significands were less than 0.1, and the area between DG c.d.f. and the diagonal was 0.21 (Fig. 5D-E, black shaded region and black data point at downward arrow, respectively). Based on calculations of area between the c.d.f.s and the diagonal line of no entrainment (Fig. 5D; Extended Data Fig. 5-1), LG was entrained by LPG at 0.03, 0.075, and 0.09 Hz ($p < 0.001$, $D > 0.303$), but not at 0.04 – 0.06 or 0.12 Hz (0.04 Hz, $p = 0.271$, $D = 0.137$; 0.05 Hz, $p = 0.689$, $D = 0.098$; 0.06 Hz, $p = 0.009$, $D = 0.226$; 0.12 Hz, $p = 0.015$, $D = 0.216$). DG was entrained by LPG at all entrainment frequencies (0.04 – 0.12 Hz, $p < 0.001$, $D > 0.45$) and IC was entrained by LPG only at 0.075 and 0.09 Hz ($p < 0.001$, $D > 0.314$), and not at the other frequencies (0.04 Hz, $p = 0.034$, $D = 0.196$; 0.05 Hz, 0.202, $D = 0.147$; 0.06 Hz, $p = 0.034$, $D = 0.196$; 0.12 Hz, $p = 0.051$, $D = 0.186$).

LPG activity is coordinated with gastric mill neurons during Gly^1-SIFamide application when only LPG synapses are functional. However, LPG was not necessary for coordinating these neurons when other chemical synapses among the gastric mill neurons were intact, suggesting overlapping functions of synaptic connections, which might interfere with measurements of the ability of LPG to entrain the other neurons (Blitz and Fahoum, 2023). Thus, we performed an additional set of experiments to directly examine whether synapses from LPG onto LG, IC, and DG neurons are functional in the presence of Gly^1-SIFamide (SIF), plus picrotoxin (PTX, 10^{-5} M; Fig. 6).

PTX application blocks glutamatergic inhibitory synapses (Bidaut, 1980), isolating LPG from the glutamatergic LG, IC, and DG gastric mill neurons. LPG uses cholinergic transmission (Marder, 1974; Hooper et al., 1986), which is not blocked by PTX. In an example experiment in the SIF:PTX condition, LPG was bursting at 0.06 Hz, and LG generated one burst at each LPG cycle (Fig. 6Ai, Baseline). When LPG was stimulated at 0.06 Hz entrainment frequency, LG maintained one burst for each LPG cycle (Fig. 6Aii). As LPG entrainment frequency was increased from 0.075 – 0.09 Hz, LG maintained 1:1 bursting with LPG, until 0.12 Hz entrainment frequency in which LG bursting became irregular (Fig. 6Aii). IC maintained a similar 1:1 bursting pattern as observed with LG across LPG entrainment frequencies (Fig. 6Bii). DG generated a burst with every other LPG cycle at baseline (Fig. 6Ci). When LPG was stimulated at entrainment frequencies of 0.06 – 0.09 Hz, DG generated 1:1 bursting with LPG, until DG bursting became irregular at 0.12 Hz entrainment frequency (Fig. 6Cii). Across experiments, many LG, IC, and DG burst frequencies occurred near entrainment mode lines, but there was still a spread of data points between entrainment modes, particularly at the lowest and highest entrainment frequencies (Fig. 6Aiii-Ciii, Table 2). Test neuron c.d.f.s in SIF:PTX (Fig. 6D) appeared larger than in Gly^1-SIFamide only (Fig. 5D). In SIF:PTX the c.d.f. histograms for LG (dark grey), IC (light grey), and DG (black) had ~50-70% of significands that were less than 0.1 at 0.06 Hz entrainment frequency (Fig. 6D, shaded regions; Extended Data Fig. 6-1). Across all entrainment frequencies, most c.d.f.s appeared to indicate greater entrainment in SIF:PTX compared to Gly^1-SIFamide alone (Extended Data Fig. 6-1 vs. Fig. 5-1). Quantitatively, LPG entrained DG between 0.04 – 0.12 Hz (Fig. 6E) ($p < 0.001$, $D > 0.39$), but not at

0.03 Hz ($p = 0.356$, $D = 0.127$). LPG was already able to entrain DG from 0.04 – 0.12 Hz in Gly^1-SIFamide (Fig. 5E), but data was not obtained at 0.03 Hz in this condition. However, for LG and IC, which were not able to be entrained by LPG from 0.04 – 0.12 Hz in Gly^1-SIFamide (Fig. 5E), LPG entrained them at all frequencies (Fig. 6E, LG, dark grey line/circles; IC, light grey line/circles) (LG:$p < 0.001$, $D > 0.27$; IC: $p < 0.001$, $D > 0.35$). Thus, it appears likely that synaptic actions from LG, IC, and/or DG in Gly^1-SIFamide interfere with the ability of LPG to control LG and IC bursting. Because only cholinergic LPG synapses were active in SIF:PTX, our entrainment assay suggests direct functional synapses from LPG onto LG, IC, and DG neurons, in the Gly^1-SIFamide modulatory state.

Altogether, the ability of LG, IC, DG, and LPG neurons to entrain one another to some extent in Gly^1-SIFamide, supports our hypothesis that typically ineffective synapses become effective during Gly^1-SIFamide application. As there is no spontaneous gastric mill rhythm in our baseline conditions, we could not use entrainment experiments to evaluate the extent to which Gly^1-SIFamide modulated connectivity between LPG and the other gastric mill neurons. For this we turned to voltage-clamp analysis of synapses. However, we first determined whether graded neurotransmission was sufficient to generate the Gly^1-SIFamide-elicited gastric mill rhythm.

Gly^1-SIFamide elicits coordinated activity among LPG, LG, IC, and DG without action potentials

Action potential (spike)-mediated and graded transmitter release are two components of neurotransmission which play complementary roles in CPG networks and are each subject to modulation (Harris-Warrick et al., 1998; Hagler et al., 2001; Beckers et al., 2009; Ivanov & Calabrese, 2006; Neff III et al., 2009; Zhao et al., 2011; Wen et al., 2013; Barnes and Kelly, 2002; Thirumalai et al., 2006). Among STG neurons, neurotransmitter release is primarily controlled in a graded, voltage-dependent manner by the subthreshold membrane potential oscillations, with some functional impact of spike-mediated transmission at a subset of synapses (Raper, 1979; Graubard et al., 1980, 1983; Thirumalai et al., 2006; Rosenbaum & Marder, 2018). In fact, CPG neurons can generate coordinated network oscillations in the absence of spike-mediated transmission under particular modulatory conditions (Raper, 1979; Harris-Warrick & Flamm, 1987; Rosenbaum & Marder, 2018). We tested whether graded transmission is also sufficient to drive the Gly^1-SIFamide gastric mill rhythm in the absence of action potentials.

In baseline Saline conditions, only the pyloric rhythm was active, with LPG and PD (*pdn*) generating pyloric-timed bursting activity (Fig. 7A, left). During application of Gly^1-SIFamide (5 µM), there was a coordinated gastric mill rhythm between LPG, LG, IC, and DG neurons (Fig. 7A, right). Spike-mediated transmission was blocked by eliminating action potential generation via application of tetrodotoxin (TTX, 0.1 µM) (Fig. 7B). During TTX plus Gly^1-SIFamide application, LPG, LG, IC, and DG generated coordinated gastric mill-timed oscillations (Fig. 7B, right; n = 2). There was coordination

of both pyloric (dotted lines) and gastric mill-timed (e.g., shaded box) oscillations between the neurons (Fig. 7B, right). Inhibitory relationships are evident for example in the most hyperpolarized membrane potentials in DG occurring during the most depolarized membrane potentials in LPG (Fig. 7B, dotted box). Thus, graded transmission is sufficient to mediate coordinated gastric-mill network activity in the Gly^1-SIFamide modulatory state.

Synaptic connections between LPG and gastric mill neurons have not been described previously. Therefore, we next examined whether graded synapses occur between LPG and the gastric mill neurons LG, IC, and DG, and whether Gly^1-SIFamide regulates the strength of any such synapses.

<u>Gly^1-SIFamide modulates synapses between LG and LPG</u>

Although our entrainment data suggest multiple synapse possibilities among LPG, LG, IC, and DG, we focused on synapses to and from LPG because we are interested in whether there is dual modulation of a switching neuron: modulation of intrinsic properties to switch neuron into a second network (Fahoum & Blitz, 2021), and modulation of synaptic properties between a switching neuron and second network neurons for coordination of switching neuron with second network (this study).

We first examined whether there was a graded synapse from LG to LPG. To test this, we applied TTX (0.1 µM, TTX:Saline) to block action potentials and recorded from LG and LPG in two-electrode voltage clamp (TEVC). LG was voltage clamped at -60 mV and stepped from -55 mV to -20 mV in 5 mV increments (5 s duration, 11 s inter-step interval) and LPG was voltage clamped at -40 mV (Fig. 8A). In TTX:Saline, there

was no apparent synaptic current elicited in LPG, suggesting that there was no functional synapse from LG to LPG in control conditions (Fig. 8A, black traces). When TTX plus Gly^1-SIFamide (TTX:Gly^1-SIFamide) was applied to the preparation, an outward current was evoked during LG voltage steps, with increased amplitude at more depolarized voltage steps (Fig. 8A, red traces). Additionally, we observed “bumps” in the LPG synaptic currents, such as in the grey trace, that were similar to transient currents that we observed between LG voltage steps (Fig. 8A, grey arrows, n = 4/4 preparations). We hypothesized that these “bumps” reflect synaptic input due to spontaneous activity in the DG and/or IC neuron. However, the early outward current (during the “first” bracket), which increased in amplitude with greater depolarization of the LG neuron, was consistently time-locked to the LG voltage steps and is thus a synaptic current elicited by depolarization of the LG neuron (Fig. 8A, red trace).To quantify the LPG response to LG voltage steps, we subtracted the mean holding current (Baseline) across two seconds immediately prior to the voltage step from the peak amplitude of LPG current at three time points: (1) first two seconds of the voltage step (First); (2) last two seconds of the voltage step (Last); and (3) first two seconds immediately after the voltage step (Post) (Fig. 8A, blue brackets). LPG synaptic current was plotted as a function of LG voltage steps and we used a two-way repeated measures (RM) ANOVA analysis with condition (TTX:Saline vs. TTX:Gly^1-SIFamide), and voltage as the two main effects, for each of the three measurement time points (Fig. 8Bi-Biii; TTX:Saline black symbols, TTX:Gly^1-SIFamide red symbols; each symbol represents one experiment). For the peak LPG synaptic current during the first 2 s, there was a significant interaction of condition and voltage (Fig. 8Bi) ($F[3,7] = 2.92$, $p =$

0.027, Two Way RM ANOVA; n = 4). Specifically, the peak current amplitude was different between TTX:Saline and TTX:Gly^1-SIFamide between -35 and -20 mV (p = 0.008 – 0.046. t = 2.32 – 3.41), except for -30 mV (p = 0.055, t = 2.20; Two Way RM ANOVA, Holm-Sidak post hoc; n = 4). Further, there was a difference in the current amplitude between some voltage steps during TTX:Gly^1-SIFamide (p < 0.001 – 0.034, t = 3.31 – 4.66) but not during TTX:Saline (p = 0.997 – 1.000, t = 0.011 – 1.35, Two Way RM ANOVA, Holm-Sidak, post hoc; n = 4). During the last 2 s of each LG voltage step, there was also a significant interaction between condition and voltage on the LPG synaptic current (Fig. 8Bii) (F[3,7] = 5.01, p = 0.002, Two Way RM ANOVA, n = 4). There was a larger LPG synaptic current during Gly^1-SIFamide compared to TTX:Saline during LG depolarizing steps from -35 to -20 mV (p < 0.001, t = 4.72 – 5.07, Two Way RM ANOVA, Holm-Sidak post hoc; n = 4). Similar to the first 2 s, there was no voltage-dependence in TTX:Saline (p = 1.000, t = 0.04 – 1.06) during the last 2 s of the voltage steps, but there were differences in the synaptic current amplitudes between some voltage steps during TTX:Gly^1-SIFamide (p < 0.001 – 0.032, t = 3.22 – 5.65, Two Way RM ANOVA, Hold-Sidak, post hoc; n = 4). Following the voltage steps (Fig. 8Biii), there was only an effect of condition with a difference between TTX:SIF and TTX:Gly^1-SIFamide (F[3,1] = 24.91, p = 0.015) but no main effect of voltage (F[3,7] = 2.34, p = 0.062), nor interaction between condition and voltage (F[3,7] = 1.31, p = 0.296, Two Way RM ANOVA; n = 4). Thus, Gly^1-SIFamide modulation enhanced a synapse from LG to LPG, which was dependent upon presynaptic voltage, that was not functional in the TTX:Saline condition.

We next tested for a synaptic connection from LPG to LG. TTX was applied with picrotoxin (PTX, 1 µM) to block LG, IC, and DG inhibitory glutamatergic synapses to examine LPG synapses onto LG that do not occur via LG, IC, or DG. Since we performed TEVC with only one of the two LPG neurons, LPG was voltage clamped at -80 mV to eliminate spontaneous bursting activity of the other non-clamped LPG neuron between voltage steps. The voltage-clamped LPG neuron was stepped from its holding voltage to -55 mV to -20 mV in 5 mV increments (5 s duration, 11 s inter-step interval) (Fig. 8C). LG was voltage clamped at -40 mV. In saline conditions, during LPG voltage steps, a series of small amplitude, inward currents were evoked in LG (Fig. 8C, black traces, black arrows). During application of Gly^1-SIFamide, there was still an initial inward current in LG within the first two seconds of each LPG voltage step, but the small repetitive currents were then summed with a larger amplitude outward current (Fig. 8C, red traces). The outward current in LG increased with increasing LPG voltage steps, indicating graded transmitter release (Fig. 8C, red traces).

We quantified LG synaptic current from LPG in the same way as described above at each of three time points, plotted LG synaptic current as a function of LPG voltage steps, and used a two-way RM ANOVA analysis comparing condition and voltage main effects for each of the three measurement time points (Fig. 8Di-Diii; TTX:Saline black symbols, TTX:Gly^1-SIFamide red symbols; each symbol represents one experiment). For the peak LG synaptic current during the first 2 s, there was no significant interaction of condition and voltage (Fig. 8Di) ($F[3,7] = 2.267$, $p = 0.069$), nor a main effect of voltage ($F[3,7] = 1.61$, $p = 0.187$) or condition ($F[3,1] = 3.95$, $p = 0.141$; Two-way RM ANOVA; $n = 4$). During the last 2 s of each LPG voltage step, there was a significant

interaction between condition and voltage (Fig. 8Dii) ($F[3,7] = 5.11$, $p = 0.002$, Two-way RM ANOVA; $n = 4$). Specifically, the peak LG synaptic current amplitude was different between TTX:Saline and TTX:Gly^1-SIFamide between -35 and -20 mV ($p = 0.029$ – 0.044, $t = 2.99$ – 3.45; Two-way RM ANOVA, Holm-Sidak post hoc; $n = 4$). Additionally, there was a difference in the synaptic current amplitude between some voltage steps during TTX:Gly^1-SIFamide ($p = 0.001$ – 0.025, $t = 3.46$ – 6.56; Two-way RM ANOVA, Holm-Sidak post hoc, $n = 4$), but not during TTX:Saline ($p = 1.000$, $t = 0.08$ – 1.0; Two-way RM ANOVA; $n = 4$). For the peak LG synaptic current during the 2 s after each LG voltage step, there was a significant interaction between condition and voltage (Fig. 8Diii) ($F[3,7] = 4.11$, $p = 0.005$, Two-way RM ANOVA; $n = 4$), such that LG synaptic current was different between TTX:Saline and TTX:Gly^1-SIFamide between -25 and -20 mV ($p = 0.027$ – 0.027, $t = 3.55$; Two-way RM ANOVA, Holm-Sidak post hoc; $n = 4$). Further, there was a difference in the synaptic current amplitude between some voltage steps during TTX:Gly^1-SIFamide ($p = 0.001$ – 0.037, $t = 3.27$ - 7.19; Two-way RM ANOVA, Holm-Sidak post hoc; $n = 4$), but not during TTX:Saline ($p = 1.000$, $t = 0.01$ - 1.25; Two-way RM ANOVA).

Unlike the outward current elicited in LG, the inward current was not voltage dependent or modulated by Gly1-SIFamide. As the inward current summed with the outward current beyond the beginning of the voltage step, we only quantified its amplitude during the initial 2 sec period. We found no interaction between condition and voltage ($F[1,7] = 0.34$, $p = 0.911$), and no effect of condition ($F[1,1] = 3.25$, $p = 0.071$) or voltage ($F[1,7] = 0.71$, $p = 0.554$; Two-way RM ANOVA, $n = 4$). In the example traces the LPG-elicited LG synaptic current (Fig. 8C) appears slower than the LG-elicited

current in LPG (Fig. 8A). This is further reflected in the small current amplitude during the initial 2 s of the steps across experiments (Fig. 8Di). In the STNS, cholinergic inhibition has a slower time course than glutamatergic inhibition (Hartline & Gassie, 1979; Eisen & Marder, 1982; Marder & Eisen, 1984; Prinz et al., 2004), aligning with the apparent differences in timing between the LG- (glutamatergic) and LPG- (cholinergic) elicited synaptic currents.

<u>Gly^1-SIFamide modulates synapses between IC and LPG</u>

We next examined whether a graded synapse was present from IC to LPG. IC was voltage clamped at -60 mV and stepped from -55 mV to -20 mV in 5 mV increments (5 s duration, 11 s inter-step interval) and LPG was voltage clamped at -40 mV (Fig. 9A, black trace). In TTX:Saline, a small outward current was elicited during steps from -35 to -20 mV indicating a functional synapse between IC and LPG in control conditions (Fig. 9A, black traces, n = 5/5). When TTX:Gly^1-SIFamide was applied to the preparation, an outward current was evoked during IC voltage steps, with increased amplitude at more depolarized voltage steps (Fig. 9A, red traces). This outward current appeared larger in amplitude than the outward current evoked in TTX:Saline, suggesting that this synapse was enhanced during Gly^1-SIFamide application. Similar to the LPG synaptic current from LG voltage steps, we observed that the LPG outward synaptic current had a steep slope as it reached its peak in the first two seconds of IC voltage steps, from -35 to -20 mV (Fig. 9A, red trace). In 5/5 preparations, we observed “bumps” in LPG synaptic current during IC voltage steps that appeared similar to those

observed during LG voltage steps (Fig. 9A, red trace, grey arrows). However, these currents occurred only during IC voltage steps, not when IC was held at -60 mV.

To quantify the LPG response to IC voltage steps, we calculated the IC-elicited synaptic current in LPG as described above at each of three time points and plotted LPG synaptic current as a function of IC voltage steps (Fig. 9Bi-Biii, TTX:Saline black symbols, TTX:Gly^1-SIFamide red symbols; each symbol represents one experiment). For the peak LPG synaptic current during the first 2 s of the IC voltage steps, there was a significant interaction of condition and voltage (Fig. 9Bi) ($F[4,7] = 3.81$, $p = 0.005$; Two-way RM ANOVA; $n = 5$). Specifically, the peak LPG current amplitude was different between TTX:Saline and TTX:Gly^1-SIFamide between -35 and -20 mV ($p = 0.007$ – 0.032, $t = 2.52$ – 3.50; Two-way RM ANOVA, Holm-Sidak post hoc; $n = 5$). In addition, there was a difference in the LPG synaptic current amplitude between some voltage steps during TTX:Gly^1-SIFamide ($p < 0.001$ – 0.022, $t = 3.47$ – 6.12), but not during TTX:Saline ($p = 0.059$ – 1.000, $t = 0.01$ – 3.28; Two-way RM ANOVA, Holm-Sidak post hoc; $n = 5$). During the last 2 s of each IC voltage step, there was also a significant interaction between condition and voltage on the LPG synaptic current (Fig. 9Bii) ($F(4, 7) = 5.07$, $p < 0.001$; Two-way RM ANOVA; $n = 5$). LPG synaptic current was larger during TTX:Gly^1-SIFamide compared to TTX:Saline during IC depolarizing voltage steps between -35 and -20 mV ($p = 0.003$ – 0.027, $t = 2.64$ – 3.96; Two-way RM ANOVA, Holm-Sidak post hoc; $n = 5$). Similar to the first 2 s, there was no voltage dependence in TTX:Saline ($p = 0.058$ – 1.000, $t = 0.05$ – 3.25) during the last 2 s of the IC voltage steps, but there were differences in the LPG synaptic current amplitudes between some voltage steps during TTX:Gly^1-SIFamide ($p < 0.001$ – 0.042, $t = 3.12$ – 7.41; Two-way

RM ANOVA, Holm-Sidak post hoc; n = 5). In the initial 2 s after the IC voltage steps (Post step), there was a significant interaction between condition and voltage on the LPG synaptic current (Fig. 9Biii) ($F[4,7] = 4.63$, $p = 0.002$; Two-way RM ANOVA; n = 5). LPG synaptic current was larger during TTX:Gly^1-SIFamide compared to TTX:Saline during IC depolarizing steps between -35 and -20 mV ($p = 0.001 – 0.021$, $t = 2.67 – 4.23$; Two-way RM ANOVA, Holm-Sidak post hoc; n = 5). Furthermore, LPG synaptic current was voltage dependent between some voltage steps during TTX:Gly^1-SIFamide ($p < 0.001 – 0.034$, $t = 3.17 – 7.87$), but not during TTX:Saline ($p = 0.155 – 1.000$, $t = 0.03 – 2.86$; Two-way RM ANOVA, Holm-Sidak post hoc; n = 5). Thus, Gly^1-SIFamide modulation enhanced a synapse from IC to LPG, which was dependent upon presynaptic voltage.

We also found a modulated synapse in the opposite direction, from LPG to IC. LPG was voltage clamped at -80 mV and stepped from -55 mV to -20 mV in 5 mV increments (5 s duration, 11 s inter-step interval) (Fig. 9C), with PTX included to block glutamatergic transmission. IC was voltage clamped at -40 mV. In saline conditions, IC responded to LPG voltage steps by generating a small amplitude, downward peak (Fig. 9C, black traces, black arrows, n = 4/5). During Gly^1-SIFamide plus TTX:PTX application, there was still an initial downward response (inward, excitatory current, n = 5/5) in the first two seconds of each LPG voltage step with a subsequent outward inhibitory current in IC that increase with more depolarized LPG voltage steps, suggesting that LPG inhibited IC in a graded manner (Fig. 9C, red traces).

Across experiments, there was an increased amplitude of LPG-elicited synaptic current in IC, with a presynaptic voltage-dependence, in Gly^1-SIFamide. For the peak IC

synaptic current in the first 2 s of each LPG voltage step, there was a significant interaction of condition and voltage (Fig. 9 Di; TTX:Saline black symbols, TTX:Gly^1-SIFamide red symbols; each symbol represents one individual) ($F[4,7] = 6.57$, $p < 0.001$; Two-way RM ANOVA; n = 5). The peak IC synaptic current amplitude was different between TTX:Saline and TTX:Gly^1-SIFamide between -50 and -20 mV ($p = 0.006 – 0.028$, $t = 3.19 – 4.90$; Two-way RM ANOVA, Holm-Sidak post hoc; n = 5). Furthermore, there was a difference in the IC current amplitude between some LPG voltage steps during TTX:Gly^1-SIFamide ($p < 0.001 – 0.027$, $t = 3.06 – 5.18$), but not during TTX:Saline ($p = 0.335 – 1.000$, $t = 0.01 – 2.53$; Two-way RM ANOVA, Holm-Sidak post hoc; n = 5). During the last 2 s of each LPG voltage step, there was also a significant interaction between condition and voltage (Fig. 9Dii) ($F[4,7] = 10.75$, $p < 0.001$; Two-way RM ANOVA; n = 5). There was a larger IC synaptic current during TTX:Gly^1-SIFamide compared to TTX:Saline during LPG depolarizing voltage steps from -55 to -20 mV ($p < 0.001 – 0.032$, $t = 2.90 – 6.93$; Two-way RM ANOVA, Holm-Sidak post hoc; n = 5). Furthermore, there was a difference in the IC synaptic current amplitude between some LPG voltage steps during TTX:Gly^1-SIFamide ($p < 0.001 – 0.047$, $t = 3.11 – 8.04$), but not during TTX:Saline ($p = 0.971 – 1.000$, $t = 0.01 – 1.59$; Two-way RM ANOVA, Holm-Sidak post hoc; n = 5). During the last 2 s of each LPG voltage step, there was also a significant interaction of condition and voltage (Fig. 9Diii) ($F[4,7] = 14.09$, $p < 0.001$; Two-way RM ANOVA; n = 5). There was a larger IC synaptic current during TTX:Gly^1-SIFamide compared to TTX:Saline during LPG depolarizing steps from -50 to -20 mV ($p = 0.001 – 0.017$, $t = 3.49 – 6.26$; Two-way RM ANOVA, Holm-Sidak post hoc; n = 5). Additionally, there were differences in the IC synaptic

current amplitudes between some LPG voltage steps during TTX:Gly^1-SIFamide ($p < 0.001 – 0.041$, $t = 2.99 – 11.07$), but not during TTX:Saline ($p = 0.993 – 1.000$, $t = 0.01 – 0.43$; Two-way RM ANOVA, Holm-Sidak post hoc; $n = 5$).

Additionally, we also measured the peak inward current in IC saline and Gly^1-SIFamide conditions. We found an effect of condition ($F[4,1] = 11.85$, $p = 0.026$) and LPG voltage ($F[4,7] = 7.13$, $p < 0.001$), but no interaction between condition and voltage ($F[4,7] = 1.28$, $p = 0.299$; Two-way RM ANOVA; $n = 5$). In conclusion, these results suggest that a voltage dependent inhibitory graded synapse from LPG onto IC was not functional in baseline condition but was enhanced by Gly^1-SIFamide modulation.

<u>Gly^1-SIFamide modulates synapses between DG and LPG</u>

Based on entrainment experiments, we predicted a stronger synapse from LPG to DG than in the other direction. DG was voltage clamped at -60 mV and stepped from -55 mV to -20 mV in 5 mV increments (5 s duration, 11 s inter-step interval) and LPG was voltage clamped at -40 mV. In an example experiment, in TTX:Saline LPG current did not appear to change relative to holding current, suggesting that there was no functional synapse between DG and LPG in control conditions (Fig. 10A, black traces). When TTX:Gly^1-SIFamide was applied to the preparation, a small outward current was evoked during DG voltage steps, but the amplitude did not appear to change with more depolarized voltage steps (Fig. 10A, red traces). Although relatively small, at more depolarized DG voltages (-25 to -20 mV), it was apparent that the LPG outward synaptic current reached its peak rapidly (Fig. 10A, red trace, $n = 3/4$), compared to the LPG to DG synaptic currents (Fig. 10C). In one preparation, there was no apparent change in

LPG synaptic current during the DG voltage steps relative to the holding current in Gly^1-SIFamide.

With one exception, DG to LPG synaptic currents were small relative to those elicited by IC and LG voltages (Figs. 8-10). Using the same quantification of synaptic currents as above, we found for the peak LPG synaptic current during the first 2 s of each DG voltage step, there was only an effect of voltage (Fig. 10Bi) ($F[3, 7] = 4.86$, $p = 0.002$, Two-way RM ANOVA; $n = 4$), such that there were differences in LPG synaptic current amplitudes between some DG voltage steps during TTX:Gly^1-SIFamide ($p < 0.001 – 0.037$, $t = 3.41 – 5.00$), but not during TTX:Saline ($p = 0.415 – 1.000$, $t = 0.02 – 2.46$; Two-way RM ANOVA, Holm-Sidak post hoc; $n = 4$). There was no effect of condition ($F[3, 1] = 4.58$, $p = 0.122$), nor interaction between condition and voltage ($F[3, 7] = 0.98$, $p = 0.475$; Two-way RM ANOVA; $n = 4$). During the last 2 s of each DG voltage step, there was an effect of voltage (Fig. 10Bii) ($F[3,7] = 6.79$, $p < 0.001$; Two-way RM ANOVA; $n = 4$), such that there were differences in LPG synaptic current amplitudes between some DG voltage steps during TTX:Gly^1-SIFamide ($p < 0.001 – 0.028$; $t = 3.46 – 6.26$), but not during TTX:Saline ($p = 0.190 – 1.000$, $t = 0.003 – 2.85$; Two-way RM ANOVA, Holm-Sidak post hoc; $n = 4$). Similar to the first 2 s, there was no effect of condition ($F[3, 1] = 5.34$, $p = 0.104$), nor an interaction between condition and voltage ($F[3, 7] = 1.88$, $p = 0.132$; Two-way RM ANOVA; $n = 4$). During the 2 s after each DG voltage step (Fig. 10Biii, Post step), there was an effect of voltage ($F[3, 7] = 4.55$, $p = 0.003$; Two-way RM ANOVA; $n = 4$), such that there were differences in LPG synaptic current amplitudes between some DG voltage steps during TTX:Gly^1-SIFamide ($p < 0.001 – 0.048$, $t = 3.31 – 5.07$), but not during TTX:Saline ($p = 0.347 – 1.000$, $t =$

0.03 – 2.57; Two-way RM ANOVA, Holm-Sidak post hoc; n = 4). There was no effect of condition (F[3, 1] = 5.18, p = 0.107), nor an interaction between condition and voltage (F[3, 7] = 1.54, p = 0.218; Two-way RM ANOVA; n = 4). Overall, although there was no statistical difference between saline and Gly^1-SIFamide conditions, there was a voltage-dependence only during Gly^1-SIFamide, which, coupled with the entrainment results, suggests that a weak DG-to-LPG synapse not effective at baseline was modulated by the peptide.

Finally, we tested whether a graded synapses from LPG to DG was present. LPG was voltage clamped at -80 mV and stepped from -55 mV to -20 mV in 5 mV increments (5 s duration, 11 s inter-step interval) (Fig. 10C). DG was voltage clamped at -40 mV. In saline conditions, DG current did not appear to change relative to holding current, suggesting that there was no functional synapse between LPG and DG in control conditions (Fig. 10C, black traces). During Gly^1-SIFamide application, DG generated an outward inhibitory current that increased with increasing LPG voltage steps, suggesting that LPG inhibited DG in a graded manner (Fig. 10C, red traces). As in LG and IC, the LPG-elicited synaptic current in DG had a slower time-course than the DG to LPG synaptic current.

Quantification and statistical analysis across experiments supported modulation of an LPG to DG synapses as in the example experiment. For the peak DG synaptic current during the first 2 s of each LPG voltage step, there was a significant interaction of condition and voltage (Fig. 10Di) (F[4, 7] = 4.45, p = 0.002; Two-way RM ANOVA; n = 5). Specifically, the peak DG synaptic current amplitude was different between TTX:Saline and TTX:Gly^1-SIFamide between -35 and -20 mV (p = 0.035 – 0.043, t =

3.00 – 2.82), except for -30 mV ($p = 0.057$, $t = 2.56$; Two-way RM ANOVA, Holm-Sidak post hoc; $n = 5$). Furthermore, there was a difference in the DG synaptic current amplitude between some LPG voltage steps during TTX:Gly^1-SIFamide ($p < 0.001$ – 0.046, $t = 3.22$ – 6.15), but not during TTX:Saline ($p = 0.998$ – 1.000, $t = 0.02$ – 0.45; Two-way RM ANOVA, Holm-Sidak post hoc; $n = 5$). During the last 2 s of each LPG voltage step, there was also a significant interaction of condition and voltage (Fig. 10Dii) ($F[4, 7] = 6.49$, $p < 0.001$; Two-way RM ANOVA; $n = 5$). There was a larger DG synaptic current during TTX:Gly^1-SIFamide compared to TTX:Saline during LPG depolarizing steps from -40 to -20 mV ($p = 0.007$ – 0.043, $t = 2.70$ – 4.41; Two-way RM ANOVA, Holm-Sidak post hoc; $n = 5$). Furthermore, there was an effect of condition $F[4, 1] = 9.90$, $p = 0.035$; Two-way RM ANOVA; $n = 5$). There was also an effect of voltage ($F[4, 7] = 6.76$, $p < 0.001$; Two-way RM ANOVA; $n = 5$), such that there were differences in DG synaptic current amplitudes between some LPG voltage steps during TTX:Gly^1-SIFamide ($p < 0.001$ – 0.023, $t = 3.37$ – 7.50), but not during TTX:Saline ($p = 1.000$, $t = 0.00006$ – 0.33; Two-way RM ANOVA, Holm-Sidak post hoc; $n = 5$). Finally, during the 2 s after each LPG voltage step (Fig. 10Diii, Post step), there was a significant interaction of condition and voltage ($F[4, 7] = 7.58$, $p < 0.001$; Two-way RM ANOVA; $n = 5$), such that there was a larger DG synaptic current during TTX:Gly^1-SIFamide compared to TTX:Saline during LPG depolarizing steps from -45 to -20 mV ($p = 0.005$ – 0.046, $t = 2.64$ – 4.80; Two-way RM ANOVA, Holm-Sidak post hoc; $n = 5$). Additionally, there was an effect of condition ($F[4, 1] = 11.21$, $p = 0.029$) and voltage ($F[4, 7] = 8.46$, $p < 0.001$; Two-way RM ANOVA; $n = 5$). Additionally, there were differences in DG synaptic current amplitudes between some LPG voltage steps during TTX:Gly^1-

SIFamide ($p < 0.001 – 0.045$, $t = 3.10 – 8.21$), but not during TTX:Saline ($p = 0.964 – 1.000$, $t = 0.05 – 0.67$; Two-way RM ANOVA, Holm-Sidak post hoc; $n = 5$). Thus, Gly^1-SIFamide modulation enhanced a synapse from LPG to DG, which was dependent upon presynaptic voltage, that was not functional in the TTX:Saline condition.

Discussion

We found entrainment among LPG, LG, IC, and DG neurons in Gly^1-SIFamide, suggesting functional synapses between multiple neuron combinations in this modulatory state. Two-electrode voltage clamp recordings confirmed that Gly^1-SIFamide enhanced connections between LPG and LG, IC, and DG (Fig. 11). This is an important complement to previously described Gly^1-SIFamide modulation of LPG intrinsic properties (Fahoum and Blitz, 2021; Snyder and Blitz, 2022).

Modulation of Internetwork Synapses

Neuromodulator regulation of synaptic strength contributes to CPG flexibility (Marder and Thirumalai, 2002; Nadim and Bucher, 2014). Previous examples identifying cellular mechanisms of neuronal switching indicate enhancement of internetwork synapses as the sole mechanism by which a neuron is both recruited to generate activity at a second frequency, and coordinated with other neurons (Hooper and Moulins, 1990; Meyrand et al., 1994; Dickinson, et al., 1990). In the control state, LPG activity is pyloric via electrical coupling with the pyloric pacemaker ensemble (Shruti et al., 2014; Fahoum and Blitz, 2021). Between gastric mill neurons and LPG, we found only a weak functional synapse from IC onto LPG. In the Gly^1-SIFamide state, LPG

switches into dual pyloric plus gastric mill-timed bursting, due to modulation of its intrinsic properties. We now show that Gly^1-SIFamide also enhances inhibitory connections between LPG and gastric mill neurons LG, IC, and DG. These modulatory actions explain the ability of LPG and LG, IC, and DG to entrain each other (this study) and to generate a coordinated rhythm (Blitz et al., 2019; Fahoum and Blitz, 2023), despite being functionally disconnected in control conditions (Fig. 11A). Thus, parallel modulatory actions impact a switching neuron such that (1) modulation of intrinsic properties enables generation of rhythmic activity at a second frequency, and (2) modulation of synaptic properties between switching and network neurons enables coordination within the second network.

Regardless of whether synaptic modulation occurs in isolation or with modulation of intrinsic properties, network output is determined by complex interactions between both sets of properties (Calabrese and Marder, 1996). Such interactions may explain the diversity of entrainment we observed. Most simply, entrainment is 1:1 coordination between two neurons, with test neuron frequency equal to entrainment frequency (Weimann et al., 1997; Thaut et al., 2015; Wilson and Cook, 2016; Marinković et al., 2020; Jiménez et al., 2022). While 1:1 entrainment among LPG, LG, IC, and DG occurred (notably from LG to IC), we also observed other coordination patterns. For instance, regardless of the entrainment neuron, DG exhibited some 1:2 entrainment (one DG burst for every two entrainment neuron bursts). In addition to LPG, DG is an endogenous burster in Gly^1-SIFamide (Fahoum and Blitz, 2023). Slower DG bursting at higher entrainment frequencies suggests that rhythmic synaptic inhibition may not be able to overcome the slower ionic currents underlying endogenous DG bursting,

reinforcing the combined contributions of synaptic and intrinsic properties to network output.

Although communication was bidirectional between all pairs, differences in synaptic properties were observed. For example, LPG cholinergic output synapses have a slower time course than glutamatergic synapses onto LPG, as do cholinergic versus glutamatergic synapses within the pyloric network (Eisen & Marder, 1982; Marder & Eisen, 1984; Prinz et al., 2004). Pharmacological block of glutamatergic transmission makes it likely that the LPG to DG synapse is direct. However, determining direct connections is difficult, even in small networks due to the complicating factor of highly prevalent electrical coupling, common across networks (Marder 2017; Nadim et al., 2017; Connors 2017). For example, LPG-elicited synaptic currents in LG and IC are difficult to interpret due to LG/IC electrical coupling. Identifying direct synapses among gastric mill neurons would require photoinactivation to selectively eliminate subsets of neurons (Eisen and Marder, 1982; Fahoum and Blitz 2021, 2023).

In addition to chemical synapses, properties of electrical synapses among gastric mill neurons are likely important in the Gly^1-SIFamide rhythm. During Gly^1-SIFamide, LG/IC gastric mill-timed bursting is typically coincident (Fahoum and Blitz, 2023), likely due to electrical coupling (Marder et al., 2017). However, while LG entrained IC in a mostly 1:1 fashion, IC only entrained LG at half of the frequencies. We speculate this difference is due to either rectifying electrical coupling, where positive current flows better from LG to IC, or an inhibitory synapse from IC to LG (Weimann and Marder, 1994) that is stronger than LG/IC electrical coupling. Rectification promotes CPG flexibility by enabling differential modulatory actions on coupled neurons, and may be

important for neuronal switching between networks (Gutierrez et al., 2013; Gutierrez & Marder, 2013; Palacios-Prado et al., 2014; Drion et al., 2019). For instance, rectifying LPG/PD electrical coupling (Shruti et al., 2014) may be important for enabling LPG switching into gastric mill timing (S-RH Fahoum, F Nadim, and DM Blitz, unpublished observations). Similarly, LG/IC rectification could enable IC recruitment from pyloric-only to dual pyloric/gastric mill timing, while preventing LG from being pulled into pyloric-timed activity. Thus, rectification can play an important role in maintaining network distinctions, even as some neurons are recruited to participate in secondary networks. Further experiments would be necessary to determine whether there is Gly^1-SIFamide modulation of electrical coupling and if present, whether it alters the extent of rectification.

<u>Functional Implications of Synaptic Modulation</u>

Synaptic modulation is a common mechanism for regulating the relative timing of neurons, and thus the particular activity pattern, although modulation of ionic currents that alter responses to synaptic input can also be important for patterning network output (Marder and Calabrese, 1996; Bucher et al., 2015; Katz 2016; Stein 2018). Other gastric mill rhythm versions are biphasic (Christie et al., 2004; Blitz et al., 2004; White and Nusbaum, 2011), whereas the Gly^1-SIFamide-elicited rhythm has a third phase, during which endogenous LPG slow bursting is out of phase with the other neurons (Fahoum and Blitz 2023). Inhibitory synapses from LPG to LG, IC, and DG likely ensure the offset between LPG and the other neurons, while synapses between LG, IC, and DG (Fig. 11B) are likely important for maintaining offsets in their timing. In fact, the

rhythm collapses into two phases (LG/IC/DG co-active and alternate with LPG) when glutamatergic synapses are blocked via PTX, leaving only cholinergic LPG synapses functional (Fahoum and Blitz 2023). Additionally, LPG regulates LG and DG neuron firing frequency in Gly^1-SIFamide (Fahoum and Blitz, 2023). Collectively, these results emphasize the full incorporation of an endogenously bursting switching neuron, such that it can actively contribute to pattern generation in a second network.

Spike-mediated and graded neurotransmission play complementary roles at vertebrate and invertebrate synapses and are both subject to neuromodulation (Johnson and Harris-Warrick, 1990; DiCaprio 2003; Alle & Geiger, 2006; Shu et al., 2006; Beckers et al., 2009; Ivanov & Calabrese, 2006; Zhao et al., 2011). In the STNS, spike-mediated and graded transmission occur, but graded is dominant and can be sufficient to generate fully coordinated pyloric rhythms under some modulatory states (Raper, 1979; Graubard et al., 1980, 1983; Rosenbaum & Marder, 2018). Here we determined that a coordinated gastric mill rhythm can occur without spike-mediated transmission in the Gly^1-SIFamide state. However, whether rhythm generating mechanisms differ for Gly^1-SIFamide compared to other gastric-mill rhythm activators, and whether they require spike-mediated transmission is unknown (Coleman et al., 1995; White and Nusbaum, 2011). Rhythm generation of episodic behaviors (e.g., chewing, locomotion) typically relies on intra-network synapses, as opposed to pacemaker neurons generating continuously active rhythms (e.g., pyloric, respiratory) (Bucher et al. 2015; Grillner and El Manira, 2020). In other gastric mill rhythm versions, reciprocal inhibition between the LG and Int1 neurons forms the core rhythm generator. Gly^1-SIFamide elicits endogenous bursting in LPG and DG, but IC and LG cannot

generate rhythmic activity in the absence of chemical synapses in Gly^{1}-SIFamide (Snyder and Blitz, 2022; Fahoum and Blitz, 2021, 2023). Thus, in addition to coordinating endogenous oscillations of the LPG switching neuron plus DG with other network neurons, the modulated graded synapses are likely necessary for rhythmic activity in at least some of the network neurons.

Conclusions

There is increasing evidence from small- to large-scale, and local to long-distance, that neuromodulators can rapidly alter network composition based on sensory information, a required behavior, or required coordination between multiple behaviors (Bartlett and Leiter, 2012; Bouret and Sara, 2005; Roopun et al., 2008; Martin and Ravel, 2014; Kopell et al., 2014; Rangel et al., 2016; van den Brink, 2019; Lohani et al., 2022). Our results indicate that parallel modulation of intrinsic and synaptic properties of a switching neuron can mediate recruiting a neuron into generating rhythmic activity at a second frequency (intrinsic properties) and coordinating those oscillations with other neurons in the network (synaptic properties), potentially providing additional flexibility under different behavioral states. It will be interesting to explore other explanations for parallel actions, such as the particular complement of intrinsic and synaptic properties that must be overcome for a switching neuron to “escape” from its home network. Thus, further investigation of cellular-level mechanisms underlying neuron recruitment into additional networks is important to gain deeper insight into the flexibility of neuronal network composition and the functional implications of neurons switching into additional networks as passive versus active members.

References

Alle H, Geiger JRP (2006) Combined analog and action potential coding in hippocampal mossy fibers. Science 311:1290–1293.

Barnes S, Kelly MEM (2002) Calcium channels at the photoreceptor synapse. Adv Exp Med and Biol 514:465–476.

Beckers U, Egelhaaf M, Kurtz R (2009) Precise timing in fly motion vision is mediated by fast components of combined graded and spike signals. Neuroscience 160:639–650.

Bidaut M (1980) Pharmacological dissection of pyloric network of the lobster stomatogastric ganglion using picrotoxin. J Neurophysiol 44:1089–1101.

Blitz DM, Christie AE, Cook AP, Dickinson PS, Nusbaum MP (2019) Similarities and differences in circuit responses to applied Gly^1-SIFamide and peptidergic (Gly^1-SIFamide) neuron stimulation. J Neurophysiol 121:950–972.

Bouret S, Sara SJ (2005) Network reset: a simplified overarching theory of locus coeruleus noradrenaline function. Trends Neurosci 28:574–582.

Bucher D, Haspel G, Golowasch J, Nadim F (2015) Central pattern generators. eLs:1-12.

Bucher D, Taylor AL, Marder E (2006) Central pattern generating neurons simultaneously express fast and slow rhythmic activities in the stomatogastric ganglion. J Neurophysiol 95:3617–3632.

Buzsáki G, Draguhn A (2004) Neuronal oscillations in cortical networks. Science 304:1926–1930.

Coleman MJ, Meyrand P, Nusbaum MP (1995) A switch between two modes of synaptic transmission mediated by presynaptic inhibition. Nature 378:502–505.

Daur N, Nadim F, Bucher D (2016) The complexity of small circuits: the stomatogastric nervous system. Curr Opin Neurobiol 41:1–7.

Devineni A V., Scaplen KM (2022) Neural circuits underlying behavioral flexibility: Insights from *Drosophila*. Front Behav Neurosci 15:1-24.

DiCaprio RA (2003) Nonspiking and spiking proprioceptors in the crab: Nonlinear analysis of nonspiking TCMRO afferents. J Neurophysiol 89:1826–1836.

Dickinson PS (1995) Interactions among neural networks for behavior. Curr Opin Neurobiol 5:792–798.

Dickinson PS, Mecsas C, Marder E (1990) Neuropeptide fusion of two motor-pattern generator circuits. Nature 344:155–157.

Dickinson PS, Stemmler EA, Cashman CR, Brennan HR, Dennison B, Huber KE, Peguero B, Rabacal W, Goiney CC, Smith CM, Towle DW, Christie AE (2008) SIFamide peptides in clawed lobsters and freshwater crayfish (Crustacea, Decapoda, Astacidea): A combined molecular, mass spectrometric and electrophysiological investigation. Gen and Comp Endocrinol 156:347–360.

Doi A, Ramirez J-M (2008) Neuromodulation and the orchestration of the respiratory rhythm. Respir Physiol Neurobiol 164:96–104.

Drion G, Franci A, Sepulchre R (2019) Cellular switches orchestrate rhythmic circuits. Biol Cybern 113:71–82.

Eisen JS, Marder E (1982) Mechanisms underlying pattern generation in lobster stomatogastric ganglion as determined by selective inactivation of identified neurons. III. Synaptic connections of electrically coupled pyloric neurons. J Neurophysiol 48:1392–1415.

Fahoum S-RH, Blitz DM (2021) Neuronal switching between single- and dual-network activity via modulation of intrinsic membrane properties. J Neurosci 41:7848–7863.

Fahoum S-RH, Blitz DM (2023) Switching neuron contributions to second network activity. bioRxiv 560974. https://doi.org/10.1101/2023.10.05.560974

Graubard K, Raper JA, Hartline DK (1980) Graded synaptic transmission between spiking neurons. PNAS 77:3733–3735.

Graubard K, Raper JA, Hartline DK (1983) Graded synaptic transmission between identified spiking neurons. J Neurophysiol 50:508–521.

Grillner S, Kozlov A (2021) The CPGs for limbed locomotion–facts and fiction. Intern J of Molec Sci 22:1-12.

Gutierrez GJ, Grashow RG (2009) *Cancer borealis* stomatogastric nervous system dissection. J Vis Exp:1–5.

Gutierrez GJ, Marder E (2013) Rectifying electrical synapses can affect the influence of synaptic modulation on output pattern robustness. J Neurosci 33:13238–13248.

Gutierrez GJ, O'Leary T, Marder E (2013) Multiple mechanisms switch an electrically coupled, synaptically inhibited neuron between competing rhythmic oscillators. Neuron 77:845–858.

Hagler DJ, And JR, Goda Y (2001) Properties of synchronous and asynchronous release during pulse train depression in cultured hippocampal neurons. J Neurophysiol 85:2324–2334.

Harris-Warrick RM, Flamm RE (1987) Multiple mechanisms of bursting in a conditional bursting neuron. J Neurosci 7:2113–2128.

Harris-Warrick RM, Johnson BR, Peck JH, Kloppenburg P, Ayali A, Skarbinski J (1998) Distributed effects of dopamine modulation in the crustacean pyloric network. Ann NY Acad Sci 860:155–167.

Hartline DK, Gassie D V (1979) Pattern generation in the lobster (*Panulirus*) stomatogastric ganglion I. Pyloric neuron kinetics and synaptic interactions. Biol Cybern 33:209-222.

Higley MJ, Cardin JA (2022) Spatiotemporal dynamics in large-scale cortical networks. Curr Op Neurobiol 77:1–7.

Hooper SL, Moulins M (1990) Cellular and synaptic mechanisms responsible for a long-lasting restructuring of the lobster pyloric network. J Neurophysiol 64:1574.

Hooper SL, O'Neil MB, Wagner R, Ewer J, Golowasch J, Marder E (1986) The innervation of the pyloric region of the crab, *Cancer borealis*: Homologous muscles in decapod species are differently innervated. J Comp Physiol A 159:227–240.

Hooper SL, Thuma JB, Guschlbauer C, Schmidt J, Büschges A (2015) Cell dialysis by sharp electrodes can cause nonphysiological changes in neuron properties. J Neurophysiol 114:1255–1271.

Huybrechts J, Nusbaum MP, Bosch L Vanden, Baggerman G, De Loof A, Schoofs L (2003) Neuropeptidomic analysis of the brain and thoracic ganglion from the Jonah crab, *Cancer borealis*. Biochem Biophys Res Commun 308:535–544.

Ivanov AI, Calabrese RL (2006) Spike-mediated and graded inhibitory synaptic transmission between leech interneurons: Evidence for shared release sites. J Neurophysiol 96:235–251.

Jiménez A, Lu Y, Jambhekar A, Lahav G (2022) Principles, mechanisms and functions of entrainment in biological oscillators. Interface Focus 12:20210088.

Johnson BR, Harris-Warrick RM (1990) Aminergic modulation of graded synaptic transmission in the lobster stomatogastric ganglion. J Neurosci 10:2066–2076.

King DG (1976) Organization of crustacean neuropil. I. Patterns of synaptic connections in lobster stomatogastric ganglion. J Neurocytol 5:207–237.

Kopell NJ, Gritton HJ, Whittington MA, Kramer MA (2014) Beyond the connectome: The dynome. Neuron 83:1319–1328.

Leiras R, Cregg JM, Kiehn O (2022) Brainstem circuits for locomotion. Ann Rev Neurosci 45:63–85.

Lohani S, Moberly AH, Benisty H, Landa B, Jing M, Li Y, Higley MJ, Cardin JA (2022) Spatiotemporally heterogeneous coordination of cholinergic and neocortical activity. Nat Neurosci 25:1706–1713.

Marder E (1974) Acetylcholine as an excitatory neuromuscular transmitter in the stomatogastric system of lobster. Nature 251:730–731.

Marder E, Bucher D (2007) Understanding circuit dynamics using the stomatogastric nervous system of lobsters and crabs. Annu Rev Physiol 69:291–316.

Marder E, Eisen JS (1984) Electrically coupled pacemaker neurons respond differently to same physiological inputs and neurotransmitters. J Neurophysiol 51:1362–1374.

Marder E, Gutierrez GJ, Nusbaum MP (2017) Complicating connectomes: Electrical coupling creates parallel pathways and degenerate circuit mechanisms. Dev Neurobiol 77:597–609.

Marder E, Thirumalai V (2002) Cellular, synaptic and network effects of neuromodulation. Neural Networks 15:479–493.

Marinković M, Berger J, Jékely G (2020) Neuronal coordination of motile cilia in locomotion and feeding. Philosoph Trans Roy Soc 375:20190165.

Meyrand P, Simmers J, Moulins M (1994) Dynamic construction of a neural network from multiple pattern generators in the lobster stomatogastric nervous system. J Neurosci 14:630–644.

Nadim F, Bucher D (2014) Neuromodulation of neurons and synapses. Curr Opin Neurobiol 29:48–56.

Nadim F, Manor Y, Nusbaum MP, Marder E (1998) Frequency regulation of a slow rhythm by a fast periodic input. J Neurosci 18:5053–5067.

Neff III RA, Conroy WG, Schoellerman JD, Berg DK (2009) Synchronous and asynchronous transmitter release at nicotinic synapses are differentially regulated by postsynaptic PSD-95 proteins. J Neurosci 29:15770–15779.

Norris BJ, Coleman MJ, Nusbaum MP (1996) Pyloric motor pattern modification by a newly identified projection neuron in the crab stomatogastric nervous system. J Neurophysiol 75:97-108.

Nusbaum MP, Beenhakker MP (2002) A small-systems approach to motor pattern generation. Nature 417:343–350.

Palacios-Prado N, Huetteroth W, Pereda AE (2014) Hemichannel composition and electrical synaptic transmission: Molecular diversity and its implications for electrical rectification. Front Cell Neurosci 8:1–13.

Powell D, Haddad SA, Gorur-Shandilya S, Marder E (2021) Coupling between fast and slow oscillator circuits in *Cancer borealis* is temperature-compensated. Elife 10.

Prinz AA, Bucher D, Marder E (2004) Similar network activity from disparate circuit parameters. Nat Neurosci 7:1345–1352.

Rangel LM, Rueckemann JW, Riviere PD, Keefe KR, Porter BS, Heimbuch IS, Budlong CH, Eichenbaum H (2016) Rhythmic coordination of hippocampal neurons during associative memory processing. Elife 5:1–24.

Raper JA (1979) Nonimpulse-mediated synaptic transmission during the generation of a cyclic motor program. Science (1979) 205:304–306.

Rosenbaum P, Marder E (2018) Graded transmission without action potentials sustains rhythmic activity in some but not all modulators that activate the same current. J Neurosci 38:8976–8988.

Schneider AC, Fox D, Itani O, Golowasch J, Bucher D, Nadim F (2021) Frequency-dependent action of neuromodulation. eNeuro 8:1-21.

Shapiro E, Castellucci VF, Kandel ER (1980) Presynaptic membrane potential affects transmitter release in an identified neuron in *Aplysia* by modulating the Ca2+ and K+ currents. PNAS 77:629–633.

Shruti S, Schulz DJ, Lett KM, Marder E (2014) Electrical coupling and innexin expression in the stomatogastric ganglion of the crab *Cancer borealis*. J Neurophysiol 112:2946–2958.

Shu Y, Hasenstaub A, Duque A, Yu Y, McCormick DA (2006) Modulation of intracortical synaptic potentials by presynaptic somatic membrane potential. Nature 441:761–765

Snyder RR, Blitz DM (2022) Multiple intrinsic membrane properties are modulated in a switch from single- to dual-network activity. J Neurophysiol 128:1181–1198.

Thaut MH, McIntosh GC, Hoemberg V (2015) Neurobiological foundations of neurologic music therapy: rhythmic entrainment and the motor system. Front Psychol 5:1-6.

Thirumalai V, Prinz AA, Johnson CD, Marder E (2006) Red pigment concentrating hormone strongly enhances the strength of the feedback to the pyloric rhythm oscillator but has little effect on pyloric rhythm period. J Neurophysiol 95:1762–1770.

Tryba AK, Peña F, Lieske SP, Viemari J-C, Thoby-Brisson M, Ramirez J-M (2008) Differential modulation of neural network and pacemaker activity underlying eupnea and sigh-breathing activities. J Neurophysiol 99:2114–2125.

van den Brink RL, Pfeffer T, Donner TH (2019) Brainstem modulation of large-scale intrinsic cortical activity correlations. Front Hum Neurosci 13:1–18.

Weimann JM, Marder E (1994) Switching neurons are integral members of multiple oscillatory networks. Curr Biol 4:896–902.

Weimann JM, Meyrand P, Marder E (1991) Neurons that form multiple pattern generators: Identification and multiple activity patterns of gastric/pyloric neurons in the crab stomatogastric system. J Neurophysiol 65:111–122.

Weimann JM, Skiebe P, Heinzel H-G, Soto C, Kopell N, Carlos Jorge-Rivera J, Marder E (1997) Modulation of oscillator interactions in the crab stomatogastric ganglion by crustacean cardioactive peptide. J Neurosci 17:1748–1760.

Wen H, Hubbard JM, Rakela B, Linhoff MW, Mandel G, Brehm P (2013) Synchronous and asynchronous modes of synaptic transmission utilize different calcium sources. Elife 2:1-19.

White RS, Nusbaum MP (2011) The same core rhythm generator underlies different rhythmic motor patterns. J Neurosci 31:11484–11494.

Wilson M, Cook PF (2016) Rhythmic entrainment: Why humans want to, fireflies can't help it, pet birds try, and sea lions have to be bribed. Psychon Bullet and Rev 23:1647–1659.

Yasuda A, Yasuda-Kamatani Y, Nozaki M, Nakajima T (2004) Identification of GYRKPPFNGSIFamide (crustacean-SIFamide) in the crayfish *Procambarus clarkii* by topological mass spectrometry analysis. Gen and Comp Endocrinol 135:391–400.

Zhao S, Sheibanie AF, Oh M, Rabbah P, Nadim F (2011) Peptide neuromodulation of synaptic dynamics in an oscillatory network. J Neurosci 31:13991–14004.

Figure Legends

Figure 1. STNS schematic and circuit diagram of pyloric and gastric mill networks.

A. The modulatory projection neuron 5 (MCN5; two copies) has a soma (arrow) in each commissural ganglion (CoG) of the stomatogastric nervous system (STNS). The axon of each MCN5 neuron projects through the inferior oesophageal (*ion*), oesophageal (*on*), and stomatogastric (*stn*) nerves and terminates in the stomatogastric ganglion (STG) to synapse with motor neurons and interneurons responsible for generating rhythmic activity of the pyloric (~1 Hz, food filtering) and gastric mill (~0.1 Hz, food chewing) feeding-related behaviors. Each pyloric and gastric mill motor neuron has axons that project through posterior motor nerves to innervate muscles that control the movements for pyloric and gastric mill activity. Vaseline wells (*circles*) were built around motor nerves to record extracellular activity of these neurons. ***B***. The circuit diagram of the STG indicates known electrical (*resistor and diode symbols*) and inhibitory chemical (*ball and stick*) synapses among pyloric and gastric mill neurons in baseline conditions. When active, the MCN5 neuron targets both pyloric and gastric mill neurons (*grey boxes*), however, synaptic modulation targets of MCN5 are unknown. Abbreviations, Ganglia: CoG, commissural ganglion; OG, oesophageal ganglion; STG, stomatogastric ganglion; Nerves: *dgn*, dorsal gastric nerve; *ion*, inferior oesophageal nerve; *lgn*, lateral gastric nerve; *lpgn* lateral posterior gastric nerve; *lvn*, lateral ventricular nerve; *mvn*, medial ventricular nerve; *on*, oesophageal nerve; *pdn*, pyloric dilator nerve; *stn*, stomatogastric nerve; *son*, superior oesophageal nerve; Neurons: AB, anterior burster; AM, anterior medial; DG, dorsal gastric; GM, gastric mill; IC, inferior cardiac; Int 1,

interneuron 1; LG, lateral gastric; LP, lateral pyloric; LPG, lateral posterior gastric; MG, medial gastric; PY, pyloric; PD, pyloric dilator; VD, ventricular dilator.

Figure 2. LG entrainment of IC, DG, and LPG gastric mill neurons during Gly^1-SIFamide application.

Ai-Ci, Aii-Cii. All columns are from the same preparation, in which LG entrainment of test neurons IC (***Ai, Aii***), DG (***Bi, Bii***), and LPG (***Ci, Cii***) was examined. In Gly^1-SIFamide (5 µM) prior to any manipulations, LG burst frequency was approximately 0.03 Hz and IC, DG, and LPG were bursting (***Ai-Ci***, Baseline). Dotted line in ***Bi*** indicates one LG cycle. ***Aii-Cii***. To determine the ability of LG to entrain the other neurons, LG was rhythmically depolarized (*upward arrowheads*, 5 s duration; LG recordings are omitted for clarity) at different entrainment frequencies, and IC (***Aii***), DG (***Bii***), and LPG (***Cii***) activity recorded. IC is active in both pyloric and gastric mill time during the Gly^1-SIFamide rhythm, but we determined the ability of only its gastric mill bursts to be entrained. IC gastric mill bursts (e.g., boxes) were identified as in previous studies (Fahoum and Blitz 2021, 2023; see Methods). ***Aiii-Ciii***. Burst frequency of IC (***Aiii***), DG (***Biii***), and LPG (***Ciii***) was plotted as a function of LG entrainment frequency. Each colored data point is one instantaneous burst frequency from one preparation. Solid diagonal line indicates perfect entrainment (1:1), where burst frequency was equal to entrainment frequency. Dashed diagonal lines indicate other modes of entrainment at which test neuron burst frequency would be a multiple, or a fraction, of entrainment frequency. Data points that fall between diagonal lines suggest a lack of LG entrainment of that neuron burst. Numbers of bursts plotted at each frequency are presented in

Table 1. ***D***. The cumulative distribution frequency (c.d.f.) of significands are overlaid for LPG (*light grey*), DG (*dark grey*), and IC (*black*) responses to an LG entrainment frequency of 0.06 Hz. Significands are the value to the right of the decimal after dividing each instantaneous burst frequency of IC, LPG, or DG by the LG entrainment frequency. Significands indicate the closeness of a ratio to an integer. The red diagonal line represents a c.d.f. where significands are randomly distributed between 0 and 1, indicating no entrainment, whereas a c.d.f. with a large portion of the distribution close to 0 and/or 1 indicates entrainment (blue dotted line). Shaded regions indicate the area between the c.d.f. for each neuron and the diagonal line. Insets of c.d.f. graphs enable visualization of area for each neuron separately ***E.*** Area between the significand c.d.f. curve and the diagonal line for IC (*black*), DG (*dark grey*), and LPG (*light grey*) as a function of LG entrainment frequency. The arrow and vertical dotted line indicate the c.d.f. area calculated for the 0.06 Hz c.d.f. histograms plotted in (***D***) (other c.d.f.s are presented in Extended Data Fig. 2-1). The dashed line at 0.25 indicates one example of perfect entrainment, calculated as the area between the dotted blue line and the red diagonal line in (***D***). The c.d.f. for each neuron at each entrainment frequency was compared to a uniform distribution indicating zero integer coupling (i.e., diagonal line) to test for statistical significance using the Kolmogorov-Smirnoff test with a corrected alpha level of 0.007 (see Methods). Area values different from the uniform distribution at each entrainment frequency are indicated above the graph for each neuron pair. *$p<0.007$, $^{ns}p>0.007$.

Figure 3. IC entrainment of LG, DG, and LPG gastric mill neurons during Gly^1-SIFamide application.

Ai-Ci, Aii-Cii. Each column panel is from one preparation, in which IC entrainment of LG (***Ai, Aii***), DG (***Bi, Bii***), and LPG (***Ci, Cii***) was examined. At baseline Gly^1-SIFamide application (5 µM), IC burst frequency was approximately 0.05 Hz and LG, DG, and LPG were bursting (***Ai-Ci***, Baseline). ***Aii-Cii***. IC was stimulated with depolarizing current injections (*upward arrowheads*, 5 s duration; IC recordings are omitted for clarity) at different entrainment frequencies, and LG (***Aii***), DG (***Bii***), and LPG (***Cii***) activity recorded. ***Aiii-Ciii***. Burst frequencies of LG (***Aiii***), DG (***Biii***), and LPG (***Ciii***) were plotted as a function of IC entrainment frequency. Each colored data point is one instantaneous burst frequency from one preparation. Solid diagonal line indicates perfect entrainment (1:1), where burst frequency was equal to entrainment frequency. Dashed diagonal lines indicate other modes of entrainment. ***D***. Overlaid cumulative distribution frequency (c.d.f.) for IC entrainment frequency of 0.06 Hz for LG (*light grey*), DG (*dark grey*), and LPG (*black*). C.d.f. was plotted as a function of the significand, which was calculated by dividing each instantaneous burst frequency of LG, LPG, or DG by the IC entrainment frequency. The red diagonal line represents a c.d.f. where significands are randomly distributed between 0 and 1, indicating no entrainment, whereas a c.d.f. with a large portion of the distribution close to 0 and/or 1 indicates entrainment (blue dotted line). Shaded regions indicate the area between the c.d.f. for each neuron and the diagonal line. Insets of c.d.f. graphs enable visualization of the area for each neuron separately. ***E.*** Area between the significand c.d.f. curve and the red diagonal line for LG (*light grey*), DG (*dark grey*), and LPG (*black*) as a function of IC entrainment frequency. The arrow

and vertical dotted line indicate the c.d.f. area calculated for the 0.06 Hz c.d.f. histograms plotted in (***D***) (other c.d.f.s are presented in Extended Data Fig. 3-1). The dashed line at 0.25 indicates one example of perfect entrainment, calculated as the area between the dotted blue line and the red diagonal line in (***D***). The c.d.f. for each neuron at each entrainment frequency was compared to a uniform distribution indicating zero integer coupling (i.e., diagonal line) to test for statistical significance using the Kolmogorov-Smirnoff test with a corrected alpha level of 0.007 (See Methods). Area values different from the uniform distribution at each entrainment frequency are indicated above the graph for each neuron pair. *$p<0.007$, $^{ns}p>0.007$.

Figure 4. **DG entrainment of LG, IC, and LPG gastric mill neurons during Gly^{1}-SIFamide application.**

Ai-Ci, Aii-Cii. Each column panel is from one preparation, in which DG entrainment of LG (***Ai, Aii***), IC (***Bi, Bii***), and LPG (***Ci, Cii***) was examined. At baseline Gly^{1}-SIFamide application (5 µM), DG burst frequency was approximately 0.04 Hz and LG, IC, and LPG were bursting (***Ai-Ci***, Baseline). ***Aii-Cii***. DG was stimulated with depolarizing current injections (*upward arrowheads*, 5 s duration; DG recording was omitted for clarity) at different entrainment frequencies, and LG, IC, and LPG activity recorded. ***Aiii-Ciii***. Burst frequency of LG (***Aiii***), IC (***Biii***), and LPG (***Ciii***) was plotted as a function of DG entrainment frequency. Each colored data point is one instantaneous burst frequency from one preparation. Solid diagonal line indicates perfect entrainment (1:1), where burst frequency was equal to entrainment frequency. Dashed diagonal lines

indicate other modes of entrainment where burst frequency was a multiple of entrainment frequency. Data points that fall between diagonal lines suggest a lack of DG entrainment of that neuron burst. ***D***. Overlaid cumulative distribution frequency (c.d.f.) for DG entrainment frequency of 0.06 Hz for LPG (*light grey*), IC (*dark grey*), and LG (*black*). C.d.f. was plotted as a function of the significand, which was calculated by dividing each instantaneous burst frequency of LG, IC, or LPG by DG entrainment frequency. The red diagonal line represents a c.d.f. where significands are randomly distributed between 0 and 1, indicating no entrainment, whereas a c.d.f. with a large portion of the distribution close to 0 and/or 1 indicates entrainment (blue dotted line). Shaded regions indicate the area between the c.d.f. for each neuron and the diagonal line. Insets of c.d.f. graphs enable visualization of the area for each neuron separately. ***E.*** Area between the significand c.d.f. curve and the diagonal line for LG (*black*), IC (*dark grey*), and LPG (*light grey*) as a function of DG entrainment frequency. The arrow and vertical dotted line indicate the c.d.f. area calculated for the 0.06 Hz c.d.f. histograms plotted in (***D***) (other c.d.f.s are presented in Extended Data Fig. 4-1). The dashed line at 0.25 indicates one example of perfect entrainment, calculated as the area between the dotted blue line and the red diagonal line in (***D)***. The c.d.f. for each neuron at each entrainment frequency was compared to a uniform distribution indicating zero integer coupling (i.e., diagonal line) to test for statistical significance using the Kolmogorov-Smirnoff test with a corrected alpha level of 0.007 (See Methods). Area values different from the uniform distribution at each entrainment frequency are indicated above the graph for each neuron pair. *$p<0.007$, $^{ns}p>0.007$.

Figure 5. LPG entrainment of LG, IC, and DG gastric mill neurons during Gly^1-SIFamide application.

Ai-Ci, Aii-Cii. Each column panel is from one preparation, in which LPG entrainment of LG (***Ai, Aii***), IC (***Bi, Bii***), and DG (***Ci, Cii***) was examined. At baseline Gly^1-SIFamide application (5 µM), LPG burst frequency was approximately 0.05 Hz and LG, IC, and DG were bursting (***Ai-Ci***, Baseline). ***Aii-Cii***. LPG was stimulated with depolarizing current injections (*upward arrowheads*, 5 s duration; LPG recording was omitted for clarity) at different entrainment frequencies, and LG (***Aii***), IC (***Bii***), and DG (***Cii***) activity recorded. ***Aiii-Ciii***. Burst frequencies of LG (***Aiii***), IC (***Biii***), and DG (***Ciii***) were plotted as a function of LPG entrainment frequency. Each colored data point is one instantaneous burst frequency from one preparation. Solid diagonal line indicates perfect entrainment (1:1), where burst frequency was equal to entrainment frequency. Dashed diagonal lines indicate other modes of entrainment where burst frequency was a multiple of entrainment frequency. Data points that fall between diagonal lines suggest a lack of LPG entrainment of that neuron burst. ***D***. Overlaid cumulative distribution frequency (c.d.f.) for LPG entrainment frequency of 0.06 Hz for IC (*light grey*), LG (*dark grey*), and DG (*black*). C.d.f. was plotted as a function of the significand, which was calculated by dividing each instantaneous burst frequency of LG, IC, or DG by LPG entrainment frequency. The red diagonal line represents a c.d.f. where significands are randomly distributed between 0 and 1, indicating no entrainment, whereas a c.d.f. with a large portion of the distribution close to 0 and/or 1 indicates entrainment (blue dotted line). Shaded regions indicate the area between the c.d.f. for each neuron and the diagonal line. Insets of c.d.f. graphs enable visualization of the area for each neuron

separately. ***E.*** Area between the significand c.d.f. curve and the diagonal line for LG (*dark grey*), IC (*light grey*), and DG (*black*) as a function of LPG entrainment frequency. The arrow and vertical dotted line indicate the c.d.f. area calculated for the 0.06 Hz c.d.f. histograms plotted in (***D***) (other c.d.f.s are presented in Extended Data Fig. 5-1). The dashed line at 0.25 indicates one example of perfect entrainment, calculated as the area between the dotted blue line and the red diagonal line in (***D)***. The c.d.f. for each neuron at each entrainment frequency was compared to a uniform distribution indicating zero integer coupling (i.e. diagonal line) to test for statistical significance using the Kolmogorov-Smirnoff test with a corrected alpha level of 0.007 (See Methods). Area values different from the uniform distribution at each entrainment frequency are indicated above the graph for each neuron pair. *$p<0.007$, $^{ns}p>0.007$.

Figure 6. **Isolated LPG entrainment of LG, IC, and DG gastric mill neurons during Gly^{1}-SIFamide plus picrotoxin (PTX, 10 µM) application (SIF:PTX).**

PTX was used to block glutamatergic inhibitory chemical synapses from LG, IC, and DG, and thus examine LPG control of LG, IC, and DG more directly. ***Ai-Ci, Aii-Cii***. Each column panel is from one preparation, in which LPG entrainment of LG (***Ai, Aii***), IC (***Bi, Bii***), and DG (***Ci, Cii***) was examined. At baseline Gly^{1}-SIFamide application (5 µM), LPG burst frequency was approximately 0.06 Hz and LG, IC, and DG were bursting (***Ai-Ci***, Baseline). ***Aii-Cii***. LPG was stimulated with depolarizing current injections (*upward arrowheads*, 5 s duration; LPG recording was omitted for clarity) at different entrainment frequencies, and LG (***Aii***), IC (***Bii***), and DG (***Cii***) activity recorded. ***Aiii-Ciii***. Burst

frequencies of LG (***Aiii***), IC (***Biii***), and DG (***Ciii***) were plotted as a function of LPG entrainment frequency. Each colored data point is one instantaneous burst frequency from one preparation. Solid diagonal line indicates perfect entrainment (1:1), where burst frequency was equal to entrainment frequency. Dashed diagonal lines indicate other modes of entrainment where burst frequency was a multiple of entrainment frequency. Data points that fall between diagonal lines suggest a lack of LPG entrainment of that neuron burst. ***D***. Overlaid cumulative distribution frequency (c.d.f.) for LPG entrainment frequency of 0.06 Hz for IC (*light grey*), LG (*dark grey*), and DG (*black*). C.d.f. was plotted as a function of the significand, which was calculated by dividing each instantaneous burst frequency of LG, IC, or DG by LPG entrainment frequency. The red diagonal line represents a c.d.f. where significands are randomly distributed between 0 and 1, indicating no entrainment, whereas a c.d.f. with a large portion of the distribution close to 0 and/or 1 indicates entrainment (blue dotted line). Shaded regions indicate the area between the c.d.f. for each neuron and the diagonal line. Insets of c.d.f. graphs enable visualization of the area for each neuron separately. Note that the shape of c.d.f. for LG, IC, and DG appear increased in SIF:PTX compared to their c.d.f. shapes In Figure 5. ***E.*** Area between the significand c.d.f. curve and the diagonal line for LG (*dark grey*), IC (*light grey*), and DG (*black*) as a function of LPG entrainment frequency. The arrow and vertical dotted line indicate the c.d.f. area calculated for the 0.06 Hz c.d.f. histograms plotted in (***D***) (other c.d.f.s are presented in Extended Data Fig. 6-1). The dashed line at 0.25 indicates one example of perfect entrainment, calculated as the area between the dotted blue line and the red diagonal line in (***D).*** The c.d.f. for each neuron at each entrainment frequency was compared to a

uniform distribution indicating zero integer coupling (i.e., diagonal line) to test for statistical significance using the Kolmogorov-Smirnoff test with a corrected alpha level of 0.007 (See Methods). Area values different from the uniform distribution at each entrainment frequency are indicated above the graph for each neuron pair. *$p<0.007$, $^{ns}p>0.007$.

Figure 7. Graded synaptic transmission is sufficient for a coordinated gastric mill rhythm in Gly^1-SIFamide.

Intracellular recordings of LPG, LG, IC, and DG during saline (*left*) and Gly^1-SIFamide application (*right*). In saline, only the pyloric rhythm was active, with LPG bursting in pyloric time with the PD neuron (*pdn*). In Gly^1-SIFamide, the gastric mill rhythm was activated (LG, DG, IC) and LPG generated both pyloric- and gastric mill-timed bursts. LPG pyloric-timed bursting in both saline and Gly^1-SIFamide was time-locked to the PD neuron *(pdn*). ***B***. Tetrodotoxin (TTX) was applied to the preparation to block action potentials (*left*), then combined with Gly^1-SIFamide (*right*). LPG, LG, IC, and DG generated gastric mill-timed oscillations in the absence of action potentials during TTX + Gly^1-SIFamide application. The shaded region indicates one gastric mill cycle, using the LG neuron as a reference neuron. Note that LG and IC were co-active and out of phase with LPG and DG neurons, as in Gly^1-SIFamide application without TTX (***A***). Troughs in DG oscillations appeared to alternate with peaks in LPG oscillations (*dotted box*). LPG, LG, and IC also generated pyloric-timed oscillations (arrows and grey lines), suggesting that Gly^1-SIFamide also activated the pyloric rhythm without action potential-mediated transmission. LPG and IC express dual-network activity while LG expresses

subthreshold pyloric-timed membrane potential changes, but fires action potentials in gastric mill time in in saline:Gly^1-SIFamide (**A**) (Fahoum and Blitz, 2021, 2023). The dotted box highlights LPG depolarization coincident with DG hyperpolarization.

Figure 8. Gly^1-SIFamide modulates graded synaptic transmission between LG and LPG.

Intracellular two-electrode voltage clamp (TEVC) recordings to examine synapses between LG and LPG. Symbols at the top indicate the synapse being tested in the left and right columns. ***A***, LPG was voltage clamped at -40 mV while LG was held at -60 mV and stepped from -55 mV to -20 mV in 5 mV increments (5 s duration, 11 s inter-step interval) in either TTX:Saline (***top***, black traces) or TTX:Gly^1-SIFamide (***bottom***, red traces). Blue brackets indicate the three time periods used for analysis in Bi-Biii/Di-Diii. Grey arrows and grey trace indicate “bumps” in LPG voltage that occurred both during and between the LG voltage steps. ***Bi-Bii***. LPG synaptic current in TTX:Saline (black) and TTX:SIF (red) as a function of LG voltage steps at each of three timepoints: First two seconds of voltage step (***Bi***), Last two seconds of voltage step (***Bii***), Post step (***Biii***). For each time point, the baseline was subtracted from the peak current within that window (blue brackets in (***A***). Different shapes in Bi-Biii and Di-Diii represent individual experiments (n = 4). Full details of two-way RM ANOVA analysis with condition (TTX:Saline vs. TTX:Gly^1-SIFamide), and voltage as the two main effects, for each of the three measurement time points for each synapse, are provided in the Results section. Briefly: ***Bi***, Saline voltage dependence, $p > 0.997$; Gly^1-SIFamide voltage dependence, $p < 0.034$; Saline versus Gly^1-SIFamide, $p < 0.046$ at -35, -25, and -20

mV; ***Bii***, Saline voltage dependence, $p = 1.000$; Gly^1-SIFamide voltage dependence, $p < 0.032$; Saline versus Gly^1-SIFamide, $p < 0.001$ between -35 and -20 mV; ***Biii***, Saline voltage dependence, $p = 1.000$; Gly^1-SIFamide voltage dependence, $p < 0.044$; Saline versus Gly^1-SIFamide, $p < 0.025$ between -35 and -20 mV. Results of two-way RM ANOVA with condition (TTX:Saline vs. TTX:Gly^1-SIFamide), and voltage as the two main effects, for each of the three measurement time points, are detailed in the Results section. ***C***. LPG was voltage clamped at -80 mV to eliminate spontaneous bursting activity of the other non-clamped LPG neuron between voltage steps and stepped to -55 mV to -20 mV in 5 mV increments (5 s duration, 11 s inter-step interval) with LG held at -40 mV. 10 µM PTX was used to block glutamatergic transmission. Synaptic currents were measued in TTX:PTX:Saline (***top*,** black traces) and TTX:PTX:Gly^1-SIFamide (***bottom***, red traces). ***Di-Dii***. LG synaptic current as a function of LPG voltage steps at each of three timepoints: First two seconds of voltage step (***Di***), Last two seconds of voltage step (***Dii***), Post step (***Diii***) (n=4). ***Di***, Saline voltage dependence, $p > 0.05$; Gly^1-SIFamide voltage dependence, $p > 0.05$; Saline versus Gly^1-SIFamide, $p = 0.069$; ***Dii***, Saline voltage dependence, $p = 1.000$; Gly^1-SIFamide voltage dependence, $p < 0.025$; Saline versus Gly^1-SIFamide, $p < 0.044$ between -35 and -20 mV; ***Diii***, Saline voltage dependence, $p > 0.999$; Gly^1-SIFamide voltage dependence, $p > 0.037$; Saline versus Gly^1-SIFamide, $p < 0.027$ between -25 and -20 mV.

Figure 9. Gly^1-SIFamide modulates graded synaptic transmission between IC and LPG.

Intracellular TEVC recordings to examine synapses between IC and LPG. Symbols at the top indicate the synapse being tested in the left and right columns. ***A***, LPG was voltage clamped at -40 mV while IC was held at -60 mV and stepped from -55 mV to -20 mV in 5 mV increments (5 s duration, 11 s inter-step interval) in either TTX:Saline (***top***, black traces) or TTX:Gly^1-SIFamide (***bottom***, red traces). Grey arrows indicate "bumps" in LPG voltage that occurred only during the IC voltage steps. ***Bi-Bii***. LPG synaptic current as a function of IC voltage steps at each of three timepoints (as indicated in Fig. 8A): First two seconds of voltage step (***Bi***), Last two seconds of voltage step (***Bii***), Post step (***Biii***). For each time point, the baseline was subtracted from the peak current within that window (blue brackets in (Fig. 8A). Different shapes in Bi-Biii and Di-Diii represent individual experiments (n = 5). Full details of two-way RM ANOVA analysis with condition (TTX:Saline vs. TTX:Gly^1-SIFamide), and voltage as the two main effects, for each of the three measurement time points for each synapse, are provided in the Results section. Briefly: ***Bi***, Saline voltage dependence, $p > 0.059$; Gly^1-SIFamide voltage dependence, $p < 0.022$; Saline versus Gly^1-SIFamide, $p < 0.032$ between -35 and -20 mV; ***Bii***, Saline voltage dependence, $p > 0.058$; Gly^1-SIFamide voltage dependence, $p < 0.042$; Saline versus Gly^1-SIFamide, $p < 0.027$ between -35 and -20 mV; ***Biii***, Saline voltage dependence, $p > 0.155$; Gly^1-SIFamide voltage dependence, $p < 0.034$; Saline versus Gly^1-SIFamide, $p < 0.021$ between -35 and -20 mV. ***C***, LPG was voltage clamped at -80 mV to eliminate spontaneous bursting activity of the other non-clamped LPG neuron between voltage steps and stepped to -55 mV to -20 mV in 5 mV

increments (5 s duration, 11 s inter-step interval) with IC held at -40 mV. 10 µM PTX was used to block glutamatergic transmission. Synaptic currents were measured in TTX:PTX:Saline (***top*****,** black traces) and TTX:PTX:Gly^1-SIFamide (***bottom***, red traces). ***Di-Dii***. IC synaptic current as a function of LPG voltage steps at each of three timepoints: First two seconds of voltage step (***Di***), Last two seconds of voltage step (***Dii***), Post step (***Diii***). ***Di***, Saline voltage dependence, $p > 0.329$; Gly^1-SIFamide voltage dependence, $p < 0.027$; Saline versus Gly^1-SIFamide, $p < 0.028$ between -50 and -20 mV; ***Dii***, Saline voltage dependence, $p > 0.971$; Gly^1-SIFamide voltage dependence, $p < 0.047$; Saline versus Gly^1-SIFamide, $p < 0.032$ between -55 and -20 mV; ***Diii***, Saline voltage dependence, $p > 0.993$; Gly^1-SIFamide voltage dependence, $p < 0.041$; Saline versus Gly^1-SIFamide, $p < 0.017$ between -50 and -20 mV.

Figure 10. Gly^1-SIFamide modulates graded synaptic transmission from LPG to DG, but not DG to LPG.

Intracellular TEVC recordings to examine synapses between DG and LPG. Symbols at the top indicate the synapse being tested in the left and right columns. ***A***, LPG was voltage clamped at -40 mV while DG was held at -60 mV and stepped from -55 mV to -20 mV in 5 mV increments (5 s duration, 11 s inter-step interval) in either TTX:Saline (***top***, black traces) or TTX:Gly^1-SIFamide (***bottom***, red traces). ***Bi-Bii***. LPG synaptic current as a function of DG voltage steps at each of three timepoints (as indicated in Fig. 8A): First two seconds of voltage step (***Bi***), Last two seconds of voltage step (***Bii***), Post step (***Biii***). For each time point, the baseline was subtracted from the peak current within that window (blue brackets in (Fig. 8A). Different shapes in Bi-Biii (n = 4) and Di-

Diii (n = 5) represent individual experiments. Full details of two-way RM ANOVA analysis with condition (TTX:Saline vs. TTX:Gly^1-SIFamide), and voltage as the two main effects, for each of the three measurement time points for each synapse, are provided in the Results section. Briefly: ***Bi***, Saline voltage dependence, $p > 0.415$; Gly^1-SIFamide voltage dependence, $p < 0.037$; Saline versus Gly^1-SIFamide, $p = 0.128$; ***Bii***, Saline voltage dependence, $p > 0.190$; Gly^1-SIFamide voltage dependence, $p < 0.028$; Saline versus Gly^1-SIFamide, $p = 0.109$; ***Biii***, Saline voltage dependence, $p > 0.347$; Gly^1-SIFamide voltage dependence, $p < 0.048$; Saline versus Gly^1-SIFamide, $p = 0.113$. Results of two-way RM ANOVA with condition (TTX:Saline vs. TTX:Gly^1-SIFamide), and voltage as the two main effects, for each of the three measurement time points, are detailed in the Results section. ***C***, LPG was voltage clamped at -80 mV to eliminate spontaneous bursting activity of the other non-clamped LPG neuron between voltage steps and stepped to -55 mV to -20 mV in 5 mV increments (5 s duration, 11 s inter-step interval) with DG held at -40 mV. 10 µM PTX was used to block glutamatergic transmission. Synaptic currents were measured in TTX:PTX:Saline (***top*,** black traces) and TTX:PTX:Gly^1-SIFamide (***bottom***, red traces). ***Di-Dii***. DG synaptic current as a function of LPG voltage steps at each of three timepoints: First two seconds of voltage step (***Di***), Last two seconds of voltage step (***Dii***), Post step (***Diii***). ***Di***, Saline voltage dependence, $p > 0.988$; Gly^1-SIFamide voltage dependence, $p < 0.046$; Saline versus Gly^1-SIFamide, $p < 0.035$ between -25 and -20 mV; ***Dii***, Saline voltage dependence, $p = 1.000$; Gly^1-SIFamide voltage dependence, $p < 0.023$; Saline versus Gly^1-SIFamide, $p < 0.043$ between -40 and -20 mV; ***Diii***, Saline voltage dependence, $p > 0.964$; Gly^1-

SIFamide voltage dependence, $p < 0.045$; Saline versus Gly^1-SIFamide, $p < 0.046$ between -45 and -20 mV.

Figure 11. Gly^1-SIFamide modulates multiple synapses.

Updated partial circuit diagram from figure 1. ***A.*** *Left,* In control conditions (Baseline), the pyloric neuron LPG is electrically coupled to the AB/PD pyloric pacemaker ensemble, and receives a weak chemical inhibitory synapse from IC. The gastric mill rhythm is off. *Right*, During Gly^1-SIFamide application, LPG intrinsic properties are modulated to enable LPG switching into dual pyloric plus gastric mill activity (red/blue LPG circle). Gly^1-SIFamide modulation also enhances bidirectional chemical inhibitory synapses between LPG and IC, LG, and DG gastric mill neurons to enable activity regulation and coordination. ***B***, Potential additional inhibitory chemical synapses that are modulated by Gly^1-SIFamide among LG, IC, and DG, based on results of entrainment experiments (Figs. 2-6). Additionally, entrainment data (Figs. 2-3) suggests that the established electrical coupling between IC and LG may be rectifying (*diode*), such that positive current flows better from LG to IC. Resistor and diode, electrical coupling; ball and stick, chemical inhibition, thickness indicates relative synapse strength; red circles, pyloric neurons; blue circles, gastric mill neurons; red/blue circles; gastropyloric neurons.

Table 1. Number of test neuron cycles per preparation from each LG, IC, and DG entrainment frequency in Gly[1]-SIFamide.

LG Entrainment Neuron				IC Entrainment Neuron				DG Entrainment Neuron			
Test Neuron	Entrain Freq (Hz)	# Cycles / Prep	*n*	Test Neuron	Entrain Freq (Hz)	# Cycles / Prep	*n*	Test Neuron	Entrain Freq (Hz)	# Cycles / Prep	*n*
IC	0.03	9-10	3	LG	0.03	--	-	LG	0.03	9-18	3
	0.04	--	-		0.04	4-22	2		0.04	12-19	4
	0.05	--	-		0.05	8-13	4		0.05	7-18	6
	0.06	8-14	7		0.06	6-11	5		0.06	5-11	8
	0.075	8-10	6		0.075	2-9	6		0.075	3-10	8
	0.09	10-11	7		0.09	5-8	4		0.09	2-9	8
	0.12	4-14	7		0.12	4-6	4		0.12	1-9	7
DG	0.03	--	-	DG	0.03	4-18	3	IC	0.03	12-14	2
	0.04	--	-		0.04	6-11	3		0.04	9-18	4
	0.05	8-9	2		0.05	9-11	3		0.05	9-17	5
	0.06	3-9	7		0.06	2-10	8		0.06	2-10	8
	0.075	2-9	6		0.075	1-10	8		0.075	6-10	7
	0.09	1-9	6		0.09	1-10	7		0.09	3-9	7
	0.12	1-9	7		0.12	1-10	7		0.12	4-7	6
LPG	0.03	23-29	3	LPG	0.03	6-28	4	LPG	0.03	15-29	3
	0.04	--	-		0.04	15-19	3		0.04	10-21	5
	0.05	14-19	2		0.05	6-12	4		0.05	6-18	6
	0.06	9-20	8		0.06	7-10	9		0.06	9-16	11
	0.075	8-10	7		0.075	3-10	9		0.075	7-14	10
	0.09	8-10	8		0.09	3-9	8		0.09	5-12	11
	0.12	5-9	8		0.12	1-11	8		0.12	4-10	11

Table 2. Number of test neuron cycles per preparation from each LPG entrainment frequency in Gly^1-SIFamide (SIF) and Gly^1-SIFamide plus PTX (SIF:PTX).

LPG Entrainment Neuron (SIF)				LPG Entrainment Neuron (SIF-PTX)			
Test Neuron	Entrain Freq (Hz)	# Cycles/ Prep	*n*	Test Neuron	Entrain Freq (Hz)	# Cycles/ Prep	*n*
LG	0.03	10-20	2	LG	0.03	11-21	4
	0.04	10-17	4		0.04	8-27	4
	0.05	9-18	5		0.05	9	3
	0.06	5-16	6		0.06	7-12	7
	0.075	5-12	6		0.075	4-9	7
	0.09	4-9	5		0.09	1-9	7
	0.12	3-10	5		0.12	1-9	7
IC	0.03	--	-	IC	0.03	7-14	4
	0.04	10-12	4		0.04	1-11	5
	0.05	9-17	5		0.05	6-10	4
	0.06	5-16	5		0.06	5-16	8
	0.075	4-12	5		0.075	1-10	8
	0.09	3-9	5		0.09	3-12	8
	0.12	3-9	5		0.12	2-8	8
DG	0.03	--	-	DG	0.03	11-16	4
	0.04	6-10	4		0.04	9-12	5
	0.05	7-12	5		0.05	9-10	4
	0.06	1-10	7		0.06	5-10	8
	0.075	2-10	7		0.075	3-9	8
	0.09	2-10	7		0.09	3-10	8
	0.12	1-10	7		0.12	2-8	7

Extended Data figure legends

Figure 2-1. LG entrainment of IC (*left*), DG (*middle*), and LPG (*right*) during Gly^1-SIFamide.

C.d.f. graphs for IC (n = 3-7), DG (n = 2-7), and LPG (n = 2-8) neurons during LG entrainment, with each row indicating the entrainment frequency. Missing graphs indicate excluded data that was n = 1, or data that was not collected for that frequency. See Table 1 for number of cycles per preparation for each neuron at each frequency.

Figure 3-1. IC entrainment of LG (*left*), DG (*middle*), and LPG (*right*) during Gly^1-SIFamide.

C.d.f. graphs for LG (n = 2-6), DG (n = 3-8), and LPG (n = 2-9) neurons during IC entrainment, with each row indicating the entrainment frequency. Missing graphs indicate excluded data that was n = 1, or data that was not collected for that frequency. See Table 1 for number of cycles per preparation for each neuron at each frequency.

Figure 4-1. **DG entrainment of LG (*left*), IC (*middle*), and LPG (*right*) during Gly^1-SIFamide.**

C.d.f. graphs for LG (n = 3-8), IC (n = 2-8), and LPG (n = 3-11) neurons during DG entrainment, with each row indicating the entrainment frequency. See Table 1 for number of cycles per preparation for each neuron at each frequency.

Figure 5-1. **LPG entrainment of LG (*left*), IC (*middle*), and DG (*right*) during Gly^{1}-SIFamide.**

C.d.f. graphs for LG (n = 2-6), IC (n = 4-5), and DG (n = 4-7) neurons during LPG entrainment, with each row indicating the entrainment frequency. Missing graphs indicate excluded data that was n = 1, or data that was not collected for that frequency. See Table 2 for number of cycles per preparation for each neuron at each frequency.

Figure 6-1. LPG entrainment of LG (*left*), IC (*middle*), and DG (*right*) during Gly^{1}-SIFamide plus picrotoxin (SIF:PTX).

C.d.f. graphs for LG (n = 4-7), IC (n = 4-8), and DG (n = 4-8) neurons during LPG entrainment, with each row indicating the entrainment frequency. See Table 2 for number of cycles per preparation for each neuron at each frequency.

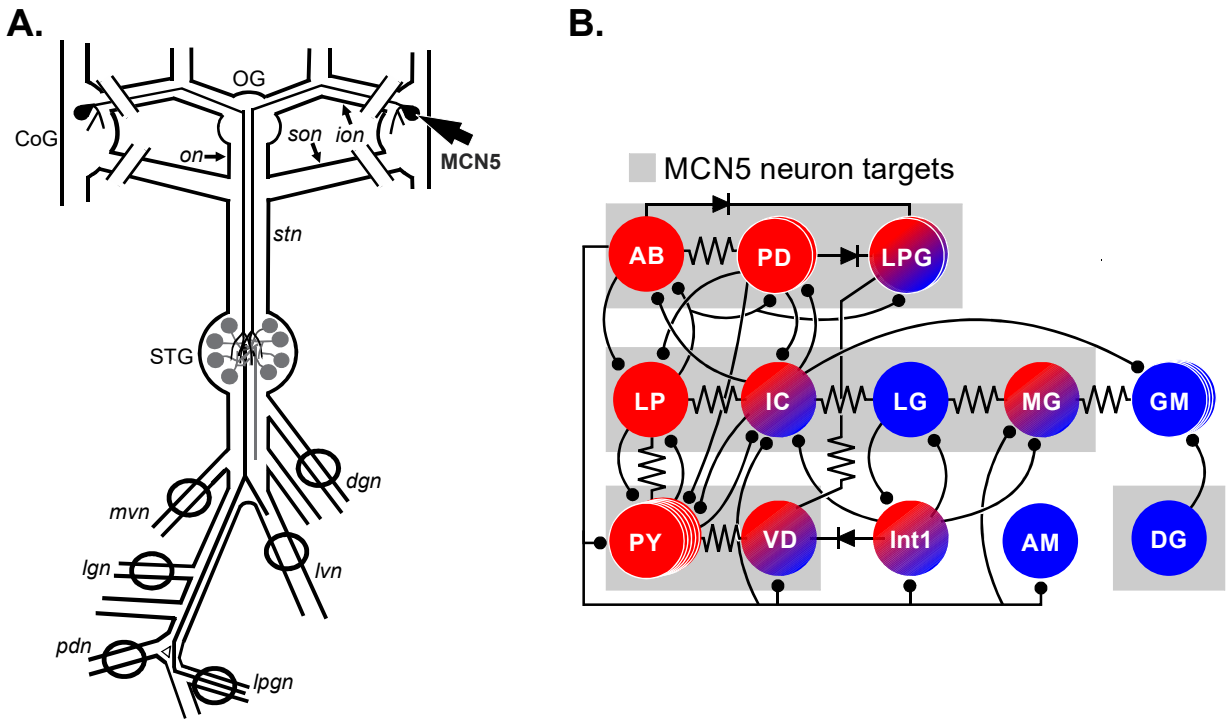

Figure 1
Fahoum and Blitz

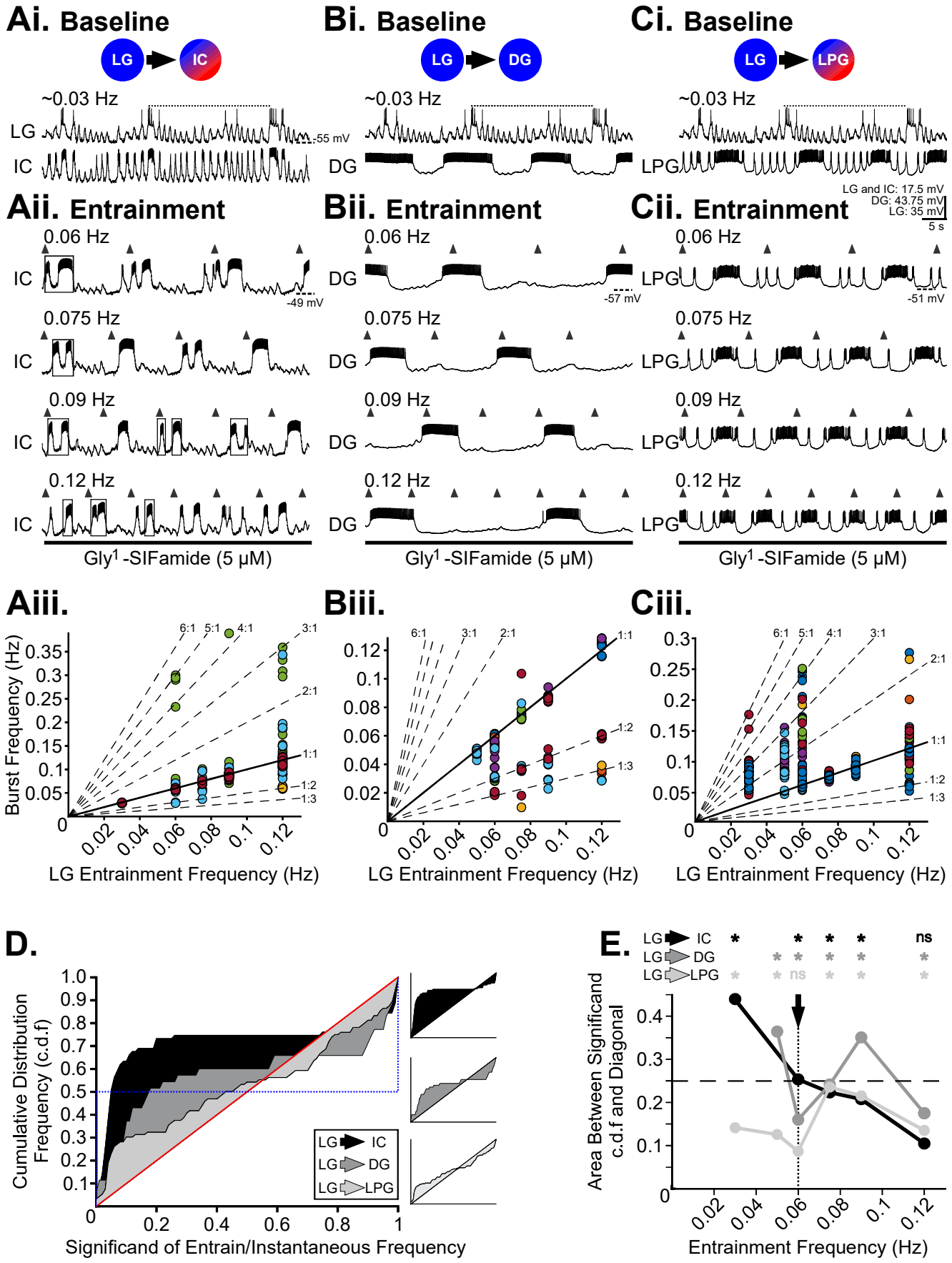

Figure 2
Fahoum and Blitz

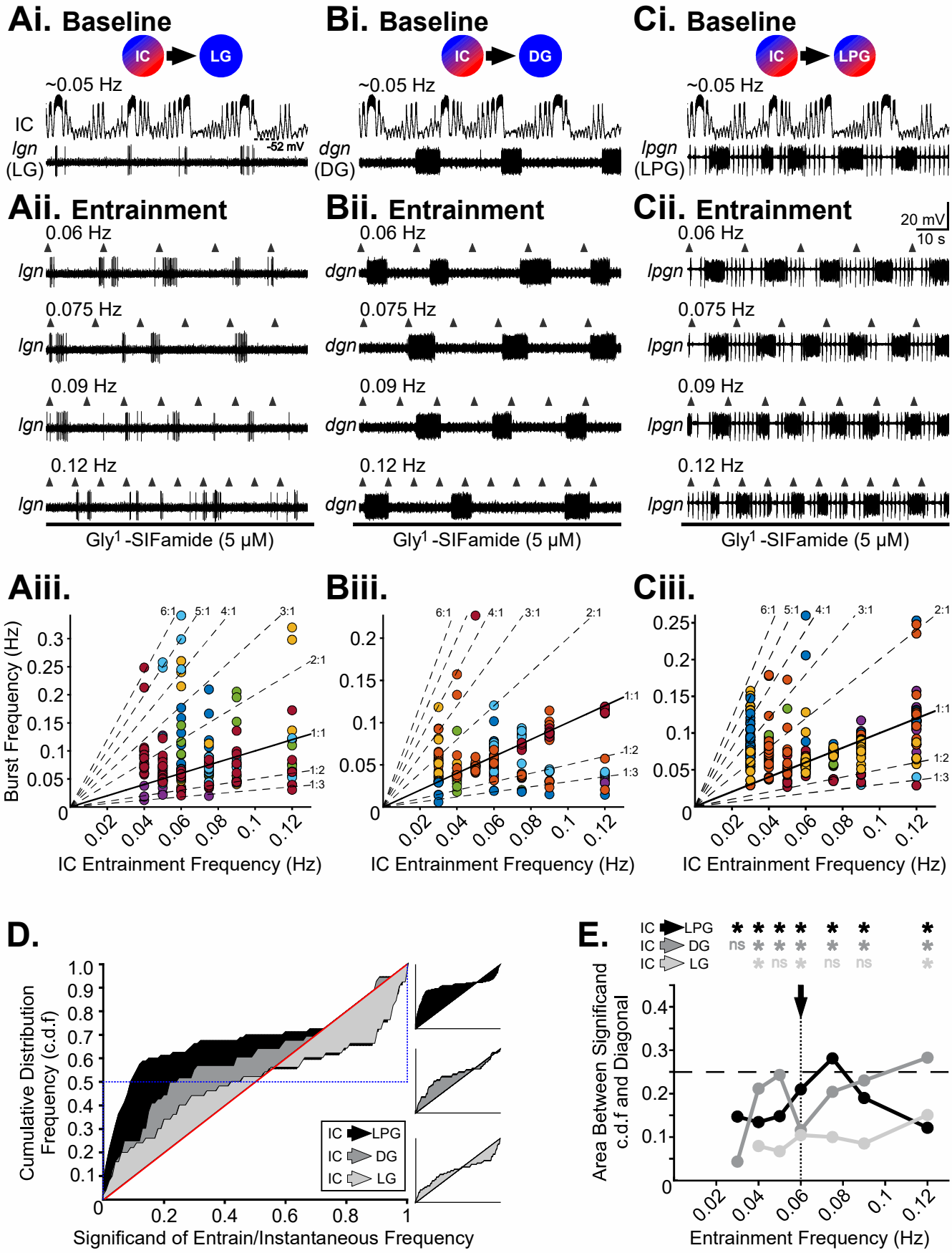

Figure 3
Fahoum and Blitz

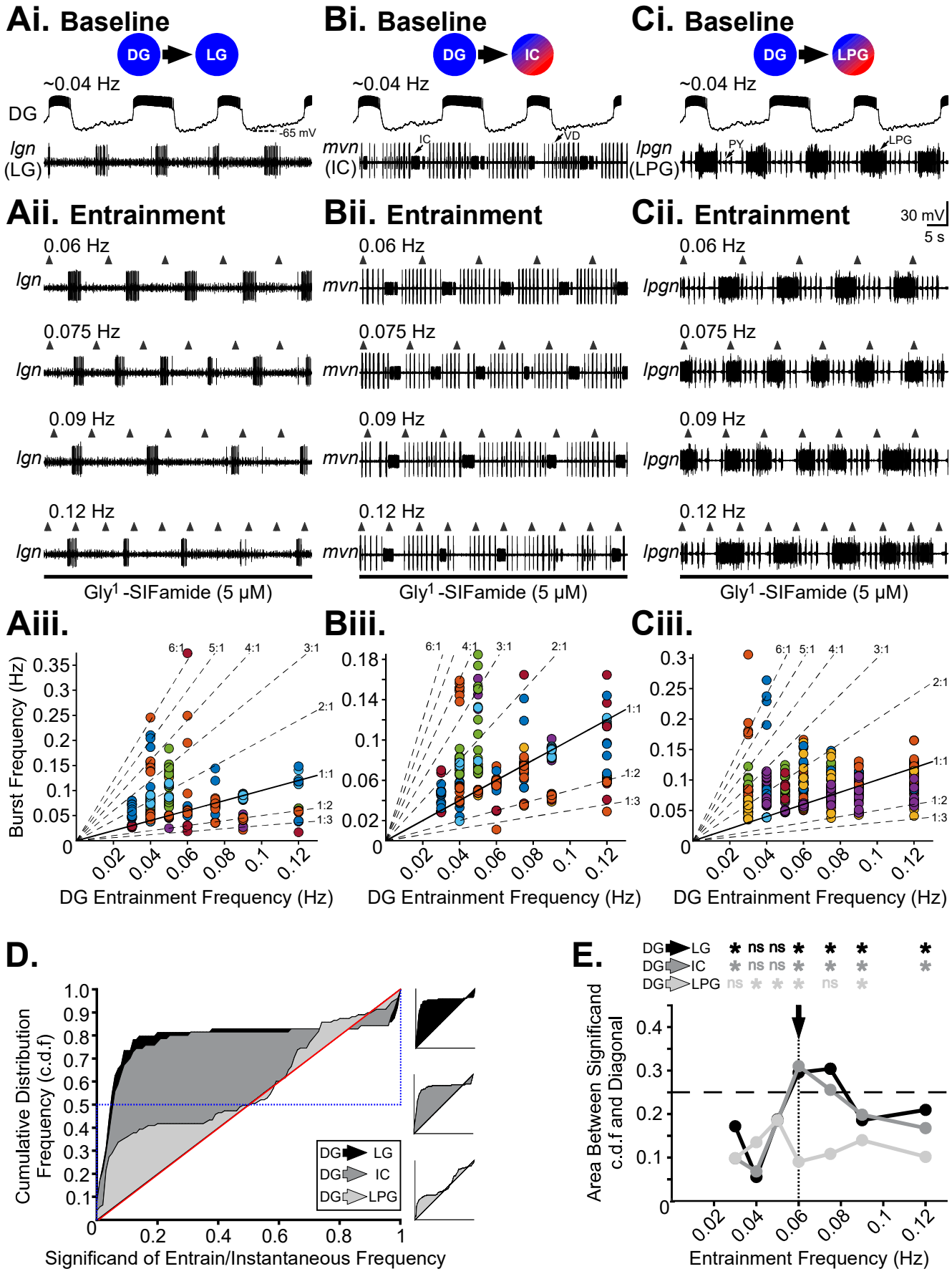

Figure 4
Fahoum and Blitz

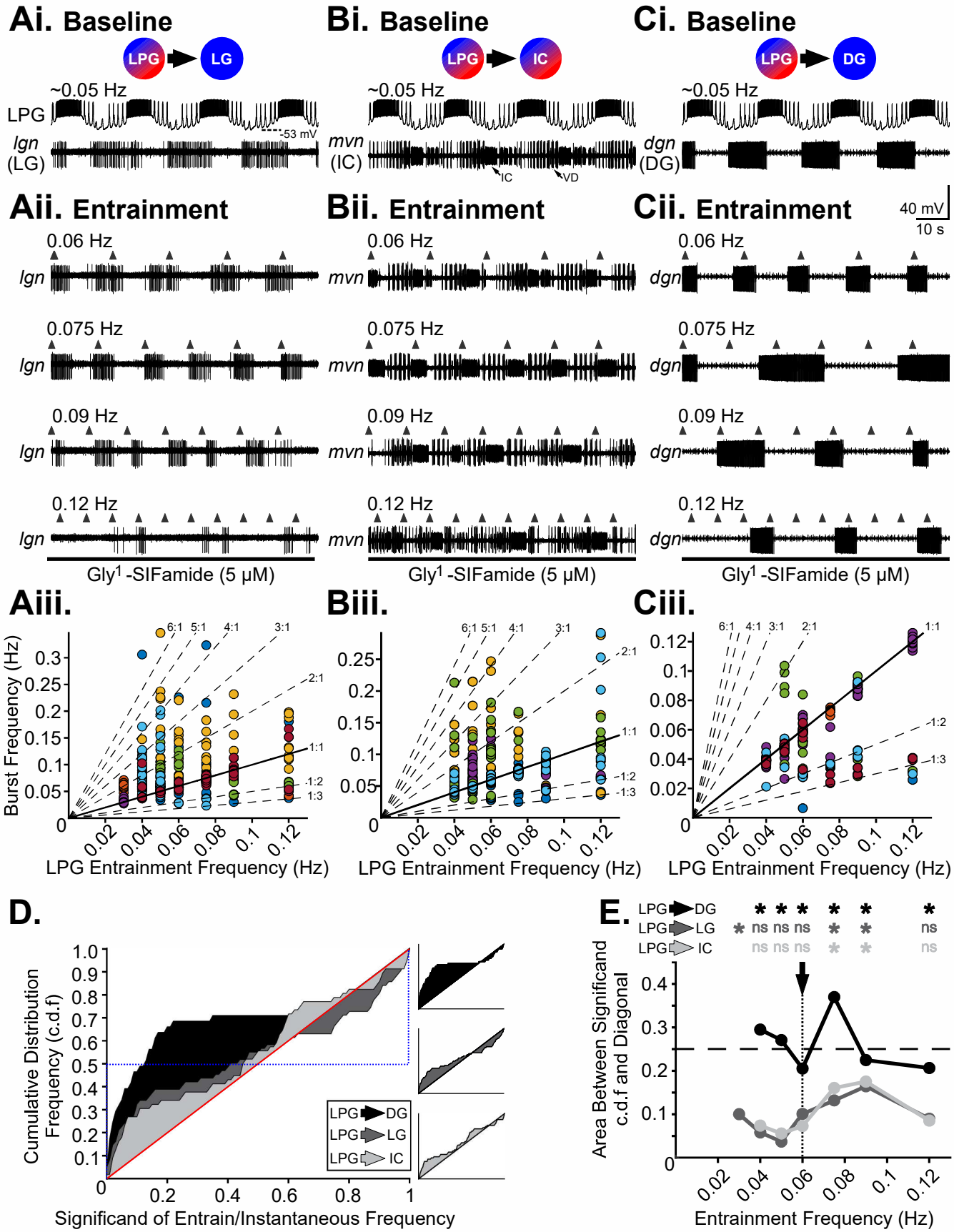

Figure 5
Fahoum and Blitz

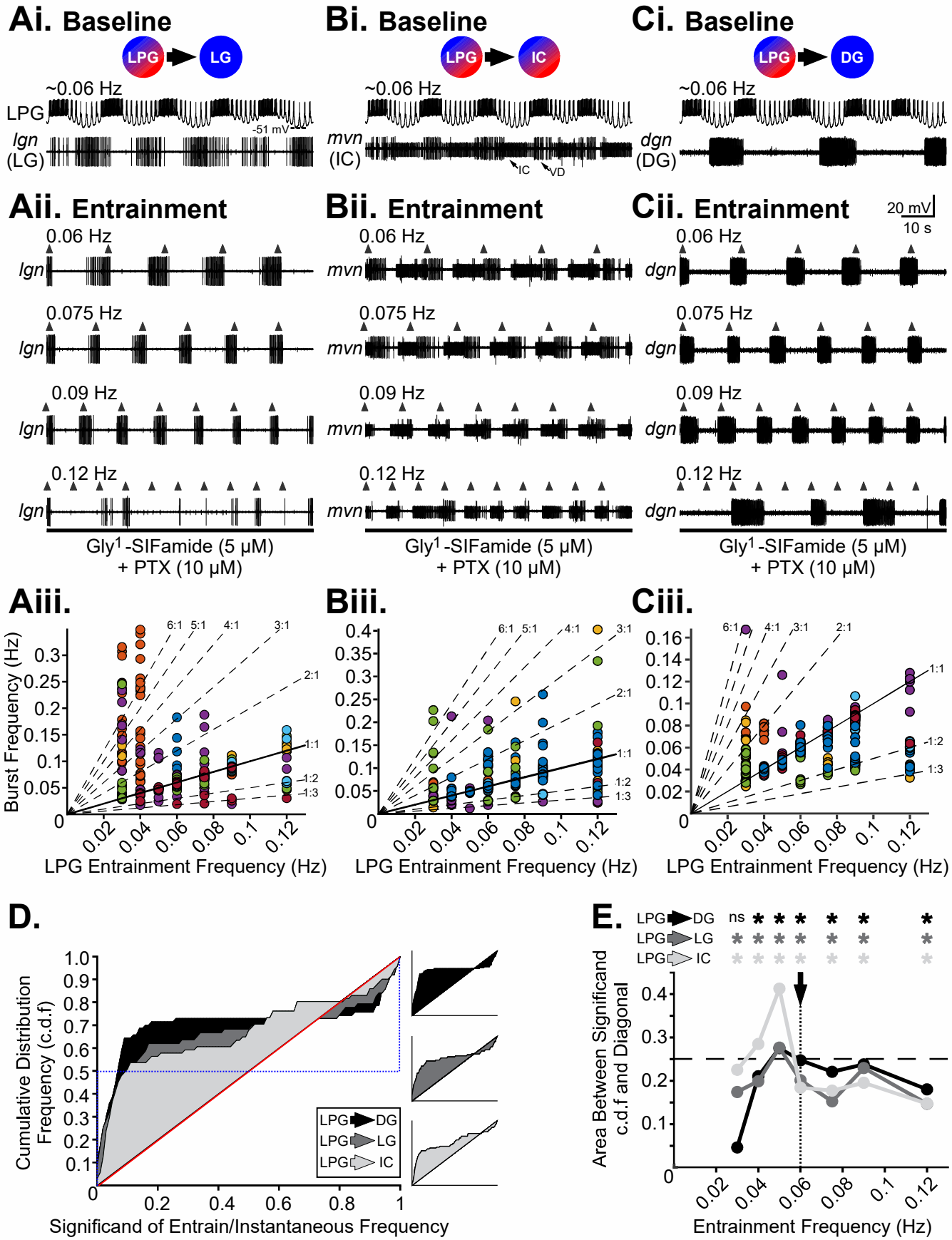

Figure 6
Fahoum and Blitz

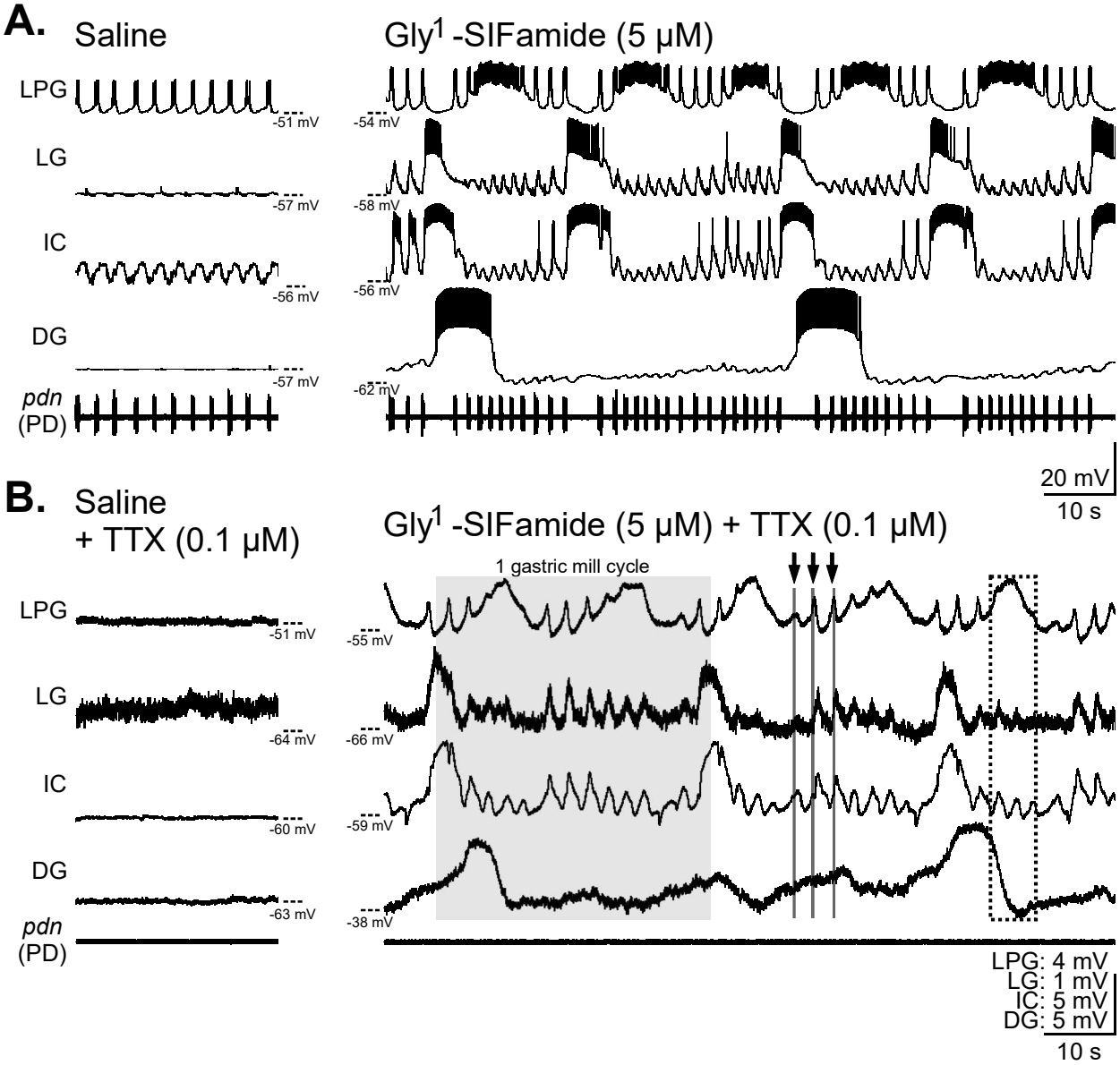

Figure 7
Fahoum and Blitz

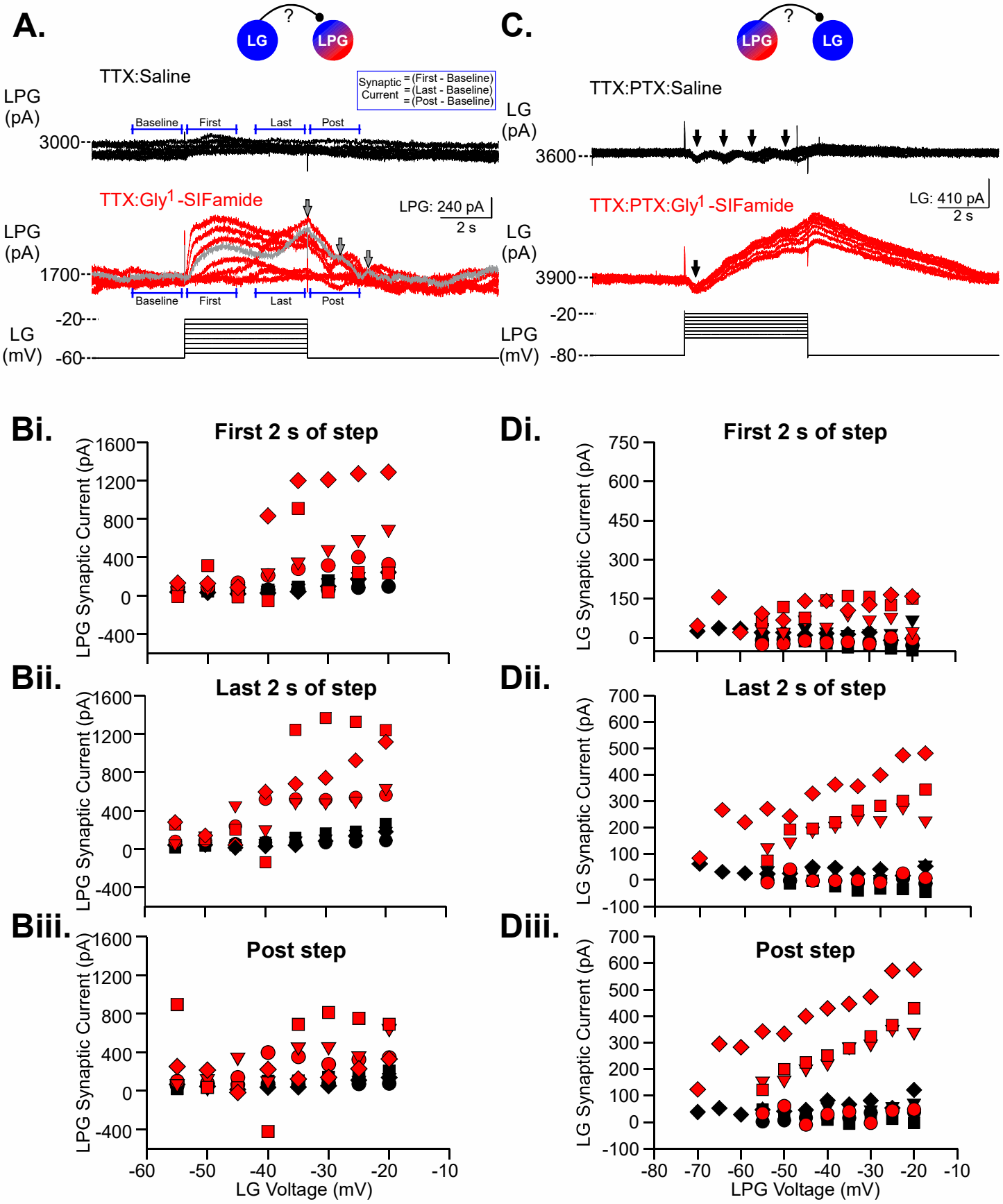

Figure 8
Fahoum and Blitz

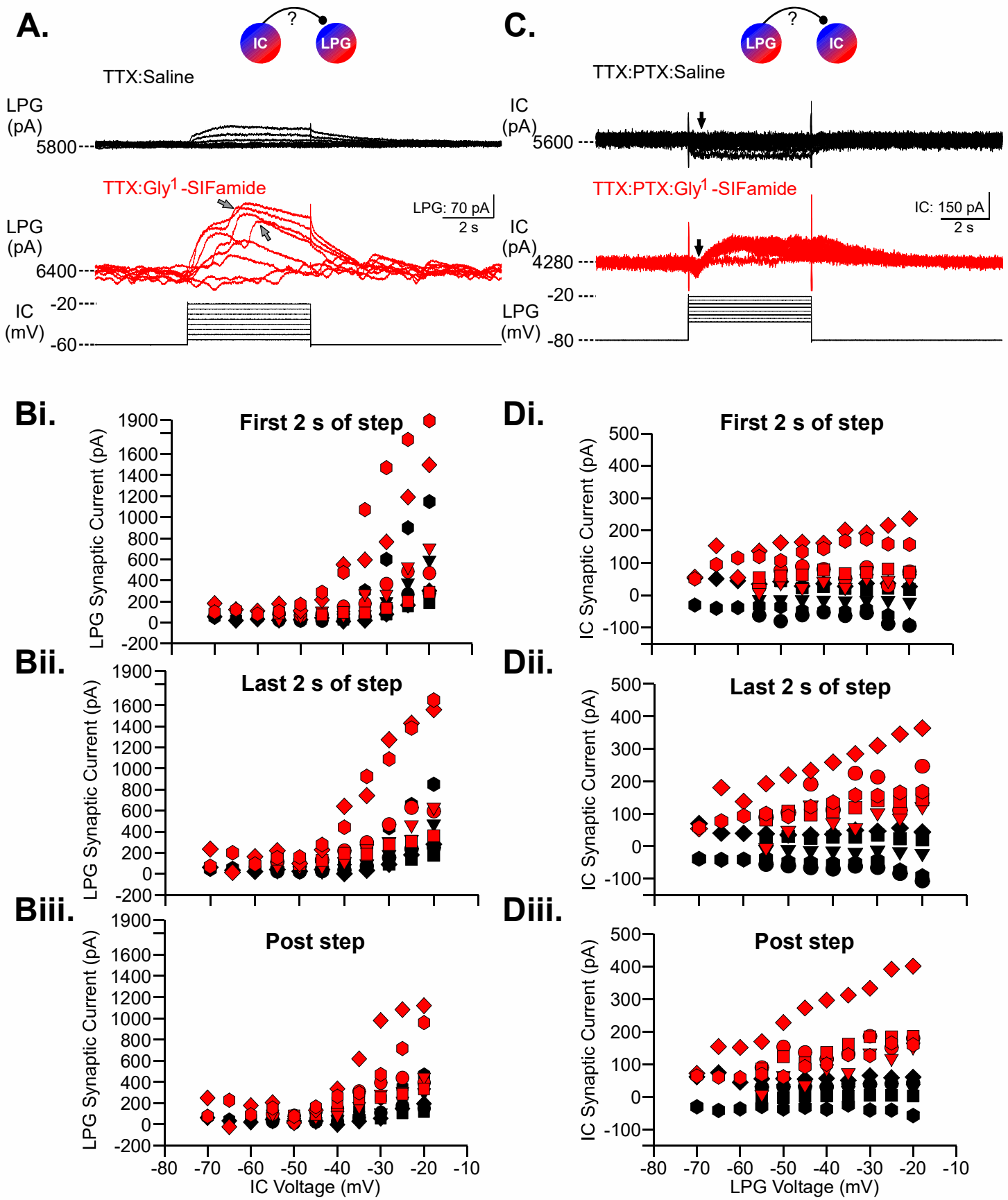

Figure 9
Fahoum and Blitz